

## Articles

**<sup>64</sup>Cu-Labeled Triphenylphosphonium and Triphenylarsonium Cations as Highly Tumor-Selective Imaging Agents**Jianjun Wang,<sup>†</sup> Chang-Tong Yang,<sup>†</sup> Young-Seung Kim,<sup>†</sup> Subramanya G. Sreerama,<sup>†</sup> Qizhen Cao,<sup>‡</sup> Zi-Bo Li,<sup>‡</sup> Zhengjie He,<sup>§</sup> Xiaoyuan Chen,<sup>‡</sup> and Shuang Liu<sup>\*,†</sup>*School of Health Sciences, Purdue University, West Lafayette, Indiana, Molecular Imaging Program at Stanford, Department of Radiology & Bio-X, Stanford University, Stanford, California, and State Key Laboratory of Elemento-Organic Chemistry, Nankai University, Tianjin 300071, P. R. China*

Received April 5, 2007

This report presents synthesis and evaluation of the <sup>64</sup>Cu-labeled triphenylphosphonium (TPP) cations as new radiotracers for imaging tumors by positron emission tomography. Biodistribution properties of <sup>64</sup>Cu-L1, <sup>64</sup>Cu-L2, <sup>64</sup>Cu-L3, and <sup>99m</sup>Tc-Sestamibi were evaluated in athymic nude mice bearing U87MG human glioma xenografts. The most striking difference is that <sup>64</sup>Cu-L1, <sup>64</sup>Cu-L2, and <sup>64</sup>Cu-L3 have much lower heart uptake (<0.6% ID/g) than <sup>99m</sup>Tc-Sestamibi (~18% ID/g) at >30 min p.i. Their tumor/heart ratios increase steadily from ~1 at 5 min p.i. to ~5 at 120 min p.i. The tumor/heart ratio of <sup>64</sup>Cu-L3 is ~40 times better than that of <sup>99m</sup>Tc-Sestamibi at 120 min postinjection. Results from in vitro assays show that <sup>64</sup>Cu-L1 is able to localize in tumor mitochondria. The tumor is clearly visualized in the tumor-bearing mice administered with <sup>64</sup>Cu-L1 as 30 min postinjection. The <sup>64</sup>Cu-labeled TPP/TPA cations are very selective radiotracers that are able to provide the information of mitochondrial bioenergetic function in tumors by monitoring mitochondrial potential in a noninvasive fashion.

**Introduction**

Alteration in the mitochondrial transmembrane potential ( $\Delta\Psi_m$ ) is an important characteristic of cancer and is caused directly by mitochondrial dysfunction, such as DNA mutation and oxidative stress.<sup>1–4</sup> It has been demonstrated that the mitochondrial transmembrane potential in carcinoma cells is significantly higher than that in normal epithelial cells.<sup>5–9</sup> For example, the difference in  $\Delta\Psi_m$  between the colon carcinoma cell line CX-1 and the control green monkey kidney epithelial cell line CV-1 was approximately 60 mV (163 mV in tumor cells versus 104 mV in normal cells). The observation that the enhanced mitochondrial transmembrane potential is prevalent in the tumor cell phenotype provides the conceptual basis for development of mitochondrion-targeting pharmaceuticals and imaging probes.<sup>1–3,10–13</sup>

Measurement of mitochondrial potential provides the most comprehensive reflection of mitochondrial bioenergetic function because it directly depends on the proper integration of diverse metabolic pathways that converge at mitochondria. Since plasma and mitochondrial transmembrane potentials are negative, delocalized cationic molecules with appropriate structural features can be driven electrophoretically through these membranes and accumulate inside the energized mitochondria.<sup>1–4,11</sup> Lipophilic organic cations, such as rhodamine-123 and <sup>3</sup>H-tetraphenylphosphonium (<sup>3</sup>H-TPP), have been widely used to measure mitochondrial potentials in tumor cells.<sup>1,14–16</sup> According to the Nernst equation, the 60 mV difference in mitochondrial transmembrane potential between the carcinoma and epithelial

cells is sufficient to account for a 10-fold greater accumulation of cationic compounds in carcinoma cells than in normal cells.<sup>1–4,11</sup> In addition, the plasma transmembrane potential (30–90 mV) can also preconcentrate the cationic species, thus affecting their cytoplasmic concentration and the availability for their mitochondrial uptake.<sup>1–4</sup>

Cationic radiotracers, such as <sup>99m</sup>Tc-Sestamibi and <sup>99m</sup>Tc-Tetrofosmin (Figure 1), originally developed as radiotracers for myocardial perfusion imaging by single photon emission computed tomography (SPECT), are also able to localize in tumor cells because of the increased mitochondrial transmembrane potential. Both <sup>99m</sup>Tc-Sestamibi and <sup>99m</sup>Tc-Tetrofosmin have been successfully used for imaging cancers and the transport function of multidrug resistance P-glycoproteins (particularly *MDR1*).<sup>17–25</sup> However, their cancer diagnostic values are often limited because of their insufficient tumor localization and high uptake in the heart and liver, which makes it very difficult to detect small lesions in the chest and abdominal regions.

More than 20 years ago, radiolabeled cations of quaternary ammonium, phosphonium and arsonium were studied as radiotracers for heart imaging.<sup>26–28</sup> Recently, several groups proposed to use the radiolabeled triphenylphosphonium (TPP) cations, such as 4-(<sup>18</sup>F-benzyl)triphenylphosphonium (Figure 1: <sup>18</sup>F-BzTPP), as positron emission tomography (PET) radiotracers for both tumor and myocardial perfusion imaging.<sup>29–37</sup> <sup>3</sup>H-Tetraphenylphosphonium (Figure 1: <sup>3</sup>H-TPP) was reported to have a better tumor uptake than <sup>99m</sup>Tc-Sestamibi, but its tumor selectivity is very poor with the tumor/heart ratio being  $\ll 1.0$ .<sup>31,35</sup> In addition, <sup>3</sup>H-TPP is not suitable for imaging purposes. The high uptake of <sup>18</sup>F-BzTPP in the heart and liver may also impose a significant challenge for its routine clinical applications in diagnosis of cancer in the chest and abdominal

\* To whom correspondence should be addressed. Phone: 765-494-0236; fax 765-496-1377; e-mail: lius@pharmacy.purdue.edu.

<sup>†</sup> Purdue University.

<sup>‡</sup> Stanford University.

<sup>§</sup> Nankai University.

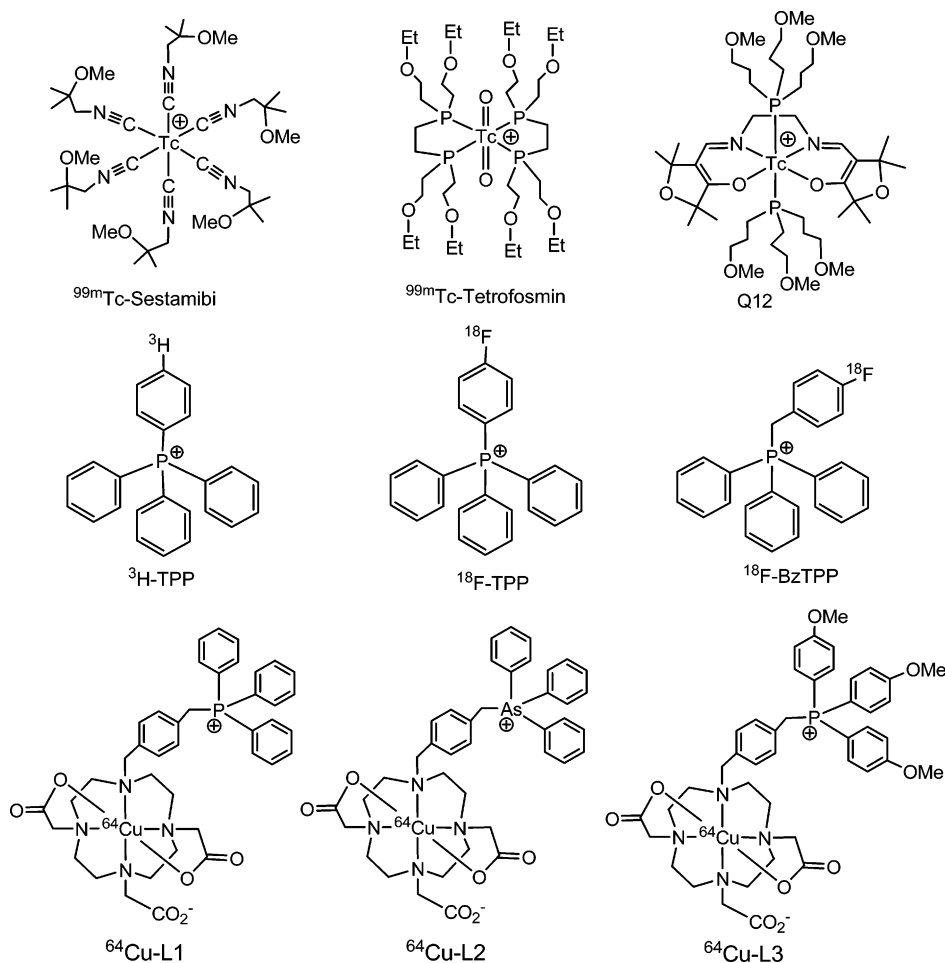


**Figure 1.** Cationic radiotracers useful for tumor imaging.  $^{99m}\text{Tc}$ -Sestamibi and  $^{99m}\text{Tc}$ -Tetrofosmin have been widely used to image tumors of different origin by SPECT.  $^{64}\text{Cu}$ -L1,  $^{64}\text{Cu}$ -L2, and  $^{64}\text{Cu}$ -L3 are evaluated in this study.

regions. Thus, there is an urgent need for new radiotracers that have high tumor-selectivity and are able to provide the information of mitochondrial bioenergetic function in tumors by monitoring mitochondrial potential in the noninvasive fashion.

Copper has several radionuclides, such as  $^{60}\text{Cu}$ ,  $^{61}\text{Cu}$ ,  $^{62}\text{Cu}$ ,  $^{64}\text{Cu}$ , and  $^{67}\text{Cu}$ . Among them,  $^{62}\text{Cu}$  and  $^{64}\text{Cu}$  are particularly useful for PET imaging.  $^{62}\text{Cu}$  has a half-life of 9.7 min and decays by positron emission (194% abundance). The short half-life of  $^{62}\text{Cu}$  allows the repeated dose without imposing a significant radiation burden to the patient.  $^{64}\text{Cu}$  has a half-life of 12.7 h and a low  $\beta^+$  emission rate (18%) with maximum  $\beta^+$  energy of 0.655 MeV. The long half-life of  $^{64}\text{Cu}$  makes it more feasible to prepare small biomolecule radiotracers. The rich coordination chemistry of copper in combination with diverse nuclear properties of its radionuclides offers many opportunities for development of diagnostic ( $^{60}\text{Cu}$ ,  $^{61}\text{Cu}$ ,  $^{62}\text{Cu}$ , and  $^{64}\text{Cu}$ ) and therapeutic ( $^{64}\text{Cu}$  and  $^{67}\text{Cu}$ ) radiotracers. Copper chemistry and radiochemistry, along with medical applications of  $^{62}\text{Cu}$ - and  $^{64}\text{Cu}$ -labeled biomolecules, have been reviewed extensively.<sup>38–41</sup>

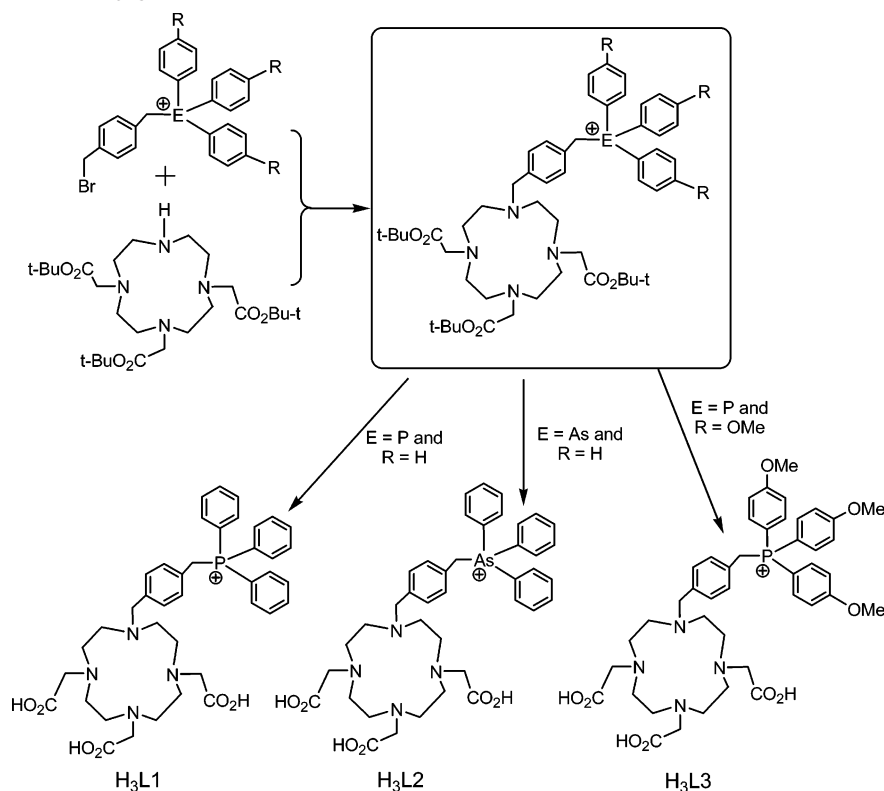
Recently, we prepared three DO3A (1,4,7,10-tetraazacyclododecane-4,7,10-triacetic acid)-conjugated TPP and triphenylarsonium (TPA) cations and their  $^{64}\text{Cu}$  complexes,  $^{64}\text{Cu}$ -L1,  $^{64}\text{Cu}$ -L2, and  $^{64}\text{Cu}$ -L3 (Figure 1). TPP or TPA acts as the “mitochondrion-targeting biomolecule” to carry  $^{64}\text{Cu}$  into tumor cells that have a much higher mitochondrial transmembrane potential than normal cells. DO3A is of particular interest as a bifunctional chelator because it is able to form a stable  $^{64}\text{Cu}$ -DO3A chelate. DO3A also forms highly stable radiometal

chelates with many other radionuclides, such as  $^{68}\text{Ga}$  for PET,  $^{111}\text{In}$  for SPECT, and  $^{90}\text{Y}$  and  $^{177}\text{Lu}$  for radiotherapy.

In this report, we present the synthesis and evaluation of  $^{64}\text{Cu}$ -L1 ( $\text{H}_3\text{L1}^a$  = triphenyl(4-((4,7,10-tris(carboxymethyl)-1,4,7,10-tetraazacyclododecan-1-yl)methyl)benzyl)phosphonium),  $^{64}\text{Cu}$ -L2 ( $\text{H}_3\text{L2}$  = triphenyl(4-((4,7,10-tris(carboxymethyl)-1,4,7,10-tetraazacyclododecan-1-yl)methyl)benzyl)arsonium), and  $^{64}\text{Cu}$ -L3 ( $\text{H}_3\text{L3}$  = tris(4-methoxyphenyl)(4-((4,7,10-tris(carboxymethyl)-1,4,7,10-tetraazacyclododecan-1-yl)methyl)benzyl)phosphonium) as new PET radiotracers for tumor imaging in athymic nude mice bearing subcutaneous U87MG human glioma xenografts. The U87MG glioma cell line was chosen because it has very limited multidrug resistance gene (particularly *MDR1*) expression.<sup>42,43</sup> We are particularly interested in the impact of heteroatoms (Figure 1: P versus As) and methoxy groups of the TPP/TPA cations on biodistribution characteristics of the corresponding  $^{64}\text{Cu}$  radiotracers. The main objective of this study is to demonstrate the intrinsic capability of the  $^{64}\text{Cu}$ -labeled TPP/TPA cations to localize in tumors. This study represents the first to use the radiometal-labeled TPP/TPA cations for tumor imaging.

<sup>a</sup> Abbreviation:  $\text{H}_3\text{L1}$ , triphenyl(4-((4,7,10-tris(carboxymethyl)-1,4,7,10-tetraazacyclododecan-1-yl)methyl)benzyl)phosphonium;  $\text{H}_3\text{L2}$ , triphenyl(4-((4,7,10-tris(carboxymethyl)-1,4,7,10-tetraazacyclododecan-1-yl)methyl)benzyl)arsonium;  $\text{H}_3\text{L3}$ , tris(4-methoxyphenyl)(4-((4,7,10-tris(carboxymethyl)-1,4,7,10-tetraazacyclododecan-1-yl)methyl)benzyl)phosphonium.

Chart 1. Synthesis of DO3A-Conjugated TPP and TPA Cations



## Experimental Section

**Materials and Instruments.** Chemicals were purchased from Sigma/Aldrich (St. Louis, MO) without further purification. DO3A-(OBu-*t*)<sub>3</sub> (1,4,7,10-tetraazacyclododecane-4,7,10-tris(*tert*-butylacetate)) was purchased from Macrocylics Inc. (Dallas, TX). The NMR (<sup>1</sup>H and <sup>13</sup>C) data were obtained using a Bruker DRX 300 MHz FT NMR spectrometer. The chemical shifts as  $\delta$  are reported in ppm relative to TMS. Infrared (IR) spectra were recorded on a Perkin-Elmer FT-IR spectrometer. Mass spectral data were collected using positive mode on a Finnigan LCQ classic mass spectrometer, School of Pharmacy, Purdue University. Elemental analysis was performed by Dr. H. Daniel Lee using a Perkin-Elmer Series III analyzer, Department of Chemistry, Purdue University. Cardiolite vials were obtained as a gift from Bristol Myers Squibb Medical Imaging (North Billerica, MA) and were reconstituted according to the manufacturer's insert. <sup>64</sup>Cu was produced using a CS-15 biomedical cyclotron at Washington University School of Medicine by the <sup>64</sup>Ni(p,n)<sup>64</sup>Cu nuclear reaction.

**HPLC Methods.** Method 1 used a LabAlliance semiprep HPLC system equipped with a UV/vis detector ( $\lambda = 254$  nm) and Zorbax C<sub>18</sub> semiprep column (9.4 mm  $\times$  250 mm, 100 Å pore size) for peptide purification. The flow rate was 2.5 mL/min. The mobile phase was isocratic with 90% solvent A (0.1% acetic acid in water) and 10% solvent B (0.1% acetic acid in acetonitrile) at 0–5 min, followed by a gradient mobile phase going from 90% solvent A and 10% solvent B at 5 min to 60% solvent A and 40% solvent B at 20 min. Method 2 used the LabAlliance HPLC system equipped with a UV/vis detector ( $\lambda = 254$  nm), a  $\beta$ -ram IN-US detector, and Vydac protein and peptide C<sub>18</sub> column (4.6 mm  $\times$  250 mm, 300 Å pore size). The flow rate was 1 mL/min with the mobile phase being isocratic with 90% solvent A (10 mM ammonium acetate) and solvent B (acetonitrile) at 0–20 min, followed by a gradient mobile phase going from 40% B at 20 min.

**(4-(Bromomethyl)benzyl)triphenylphosphonium Bromide.** Triphenylphosphine (0.54 g, 2 mmol) was dissolved in toluene (6 mL), and the resulting solution was added dropwise to a toluene solution (5 mL) containing  $\alpha,\alpha'$ -dibromomethyl-*p*-xylene (0.53 g, 2 mmol) at 100 °C. The mixture was refluxed at 100 °C for 18 h.

The white solid was filtered, washed with toluene (5 mL) and diethyl ether (20 mL), and then dried under vacuum to give the intermediate product: (4-(bromomethyl)benzyl)triphenylphosphonium bromide. The yield was 0.93 g (88.4%). <sup>1</sup>H NMR (CDCl<sub>3</sub>, chemical shift  $\delta$  in ppm relative to TMS): 4.35 (s, 2H, CH<sub>2</sub>Br), 5.48 (d, 2H, PCH<sub>2</sub>, *J*<sub>PH</sub> = 15 Hz), 7.09 (m, 4H, C<sub>6</sub>H<sub>4</sub>), 7.74–7.55 (m, 15H, C<sub>6</sub>H<sub>5</sub>). ESI-MS: *m/z* = 446.3 for [M + H]<sup>+</sup> (calcd 446 for [C<sub>26</sub>H<sub>23</sub>-PBr]<sup>+</sup>).

**(4-(Bromomethyl)benzyl)triphenylarsonium Bromide.** Triphenylarsine (0.90 g, 3.0 mmol) and  $\alpha,\alpha'$ -dibromomethyl-*p*-xylene (0.87 g, 3.3 mmol) were dissolved in nitromethane (8 mL). The resulting solution was refluxed for 6 h. The mixture was cooled to room temperature and kept still overnight to afford a white solid. After filtration, the white solid was washed with a small amount of acetone and dried under vacuum overnight. The yield was 0.41 g (24%). <sup>1</sup>H NMR (CDCl<sub>3</sub>): 7.69–7.53 (m, 19H), 7.07 (s, 2H), 5.48 (s, 2H). ESI-MS: *m/z* = 490.3 for [M + H]<sup>+</sup> (calcd 490 for [C<sub>26</sub>H<sub>23</sub>AsBr]<sup>+</sup>).

**(4-(Bromomethyl)benzyl)tris(4-methoxyphenyl)phosphonium Bromide.** Tris(4-methoxyphenyl)phosphine (0.74 g, 2.0 mmol) was dissolved in toluene (6 mL). The resulting solution was added dropwise to a toluene solution (5 mL) containing  $\alpha,\alpha'$ -dibromo-*p*-xylene (0.53 g, 2.0 mmol) at 100 °C. After the reaction mixture was refluxed at 100 °C for 18 h, the white solid was filtered, washed with toluene (5 mL) and diethyl ether (20 mL), and then dried under vacuum to give the product: (4-(bromomethyl)benzyl)tris(4-methoxyphenyl)phosphonium bromide. The yield was 1.02 g (84.2%). <sup>1</sup>H NMR (CDCl<sub>3</sub>, chemical shift  $\delta$  in ppm relative to TMS): 3.86 (s, 9H, 4-OCH<sub>3</sub>); 4.36 (s, 2H, CH<sub>2</sub>Br); 5.08 (d, 2H, PCH<sub>2</sub>, *J*<sub>PH</sub> = 15 Hz); 6.86–7.63 (m, 16H aromatic). ESI-MS: *m/z* = 536.4 for [M<sup>+</sup> + H] (calcd 536 for [C<sub>29</sub>H<sub>29</sub>O<sub>3</sub>PBr]<sup>+</sup>). The intermediate product was used for the next step reaction without further purification.

**Triphenyl(4-((4,7,10-tris(carboxymethyl)-1,4,7,10-tetraazacyclododecan-1-yl)methyl)benzyl)phosphonium (H<sub>3</sub>L1).** Triethylamine (0.5 mmol) was added to a solution of (4-(bromomethyl)benzyl)triphenylphosphonium bromide (52.6 mg, 0.1 mmol) and DO3A(OBu-*t*)<sub>3</sub> (52.0 mg, 0.1 mmol) in 3 mL of anhydrous DMF. The mixture was stirred overnight at room temperature. Upon

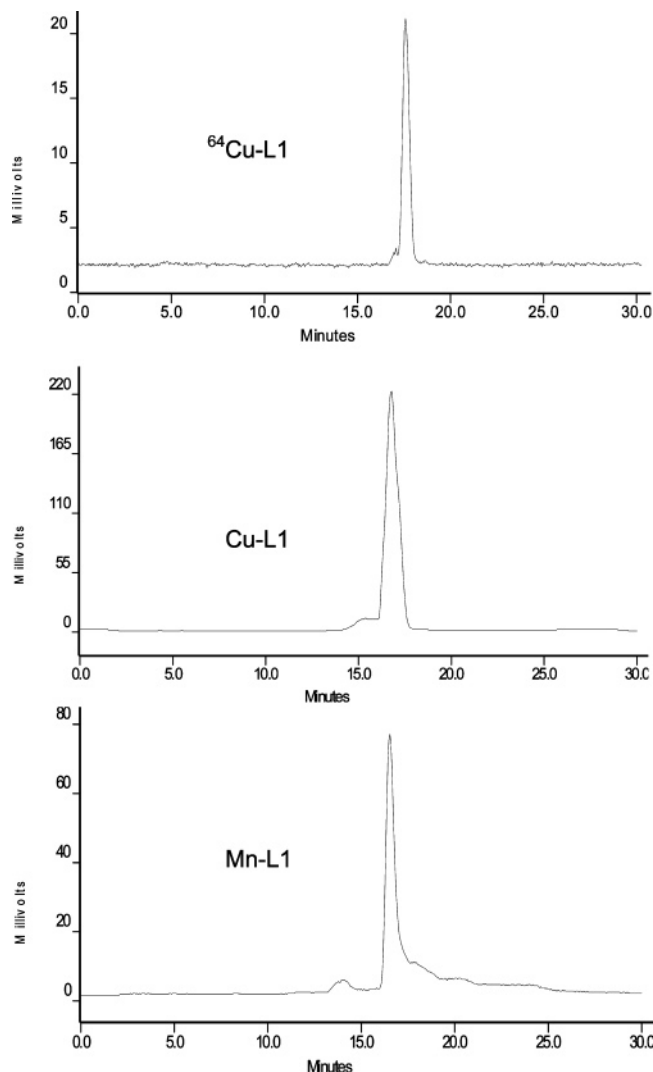


**Figure 2.** Representative HPLC chromatograms of  $^{64}\text{Cu}$ -L1, Cu-L1, and Mn-L1 under identical chromatographic conditions. Their almost identical HPLC retention times suggest that the same metal complex was prepared at the tracer ( $^{64}\text{Cu}$ ) and macroscopic (Cu) levels, and that Cu-L1 most likely exists as its zwitterion form as observed for Mn-L1.

removal of DMF and excess triethylamine under reduced pressure, the residue was dissolved in 2 mL of concentrated HCl. After being stirred at room temperature for 10–20 min, volatiles were removed under the reduced pressure. The residue was dissolved in 4 mL of 50% DMF/water mixture, and the product was separated by HPLC. Fractions at  $\sim 16.5$  min were collected and lyophilized to give a white powder. The yield was 45 mg (63%). The HPLC retention time was  $\sim 16.5$  min (Method 1) with purity  $>98\%$ .  $^1\text{H}$  NMR ( $\text{D}_2\text{O}$ , chemical shift  $\delta$  in ppm relative to TMS): 2.80–3.7 (m, 22H), 4.63 (s, 2H,  $\text{CH}_2$ ), 4.68 (d, 2H,  $\text{PCH}_2$ ,  $J_{\text{PH}} = 13$  Hz), 6.86–7.75 (m, 19H, aromatic). ES-MS:  $m/z = 711.3$  for  $[\text{M} + \text{H}]^+$  (calcd 711 for  $[\text{C}_{40}\text{H}_{48}\text{N}_4\text{O}_6\text{P}]^+$ ). Anal. Calcd for  $\text{C}_{42}\text{H}_{51}\text{N}_4\text{O}_8\text{P}\cdot 4\text{H}_2\text{O}$ : C, 59.85; H, 7.06; N, 6.65. Found: C, 59.53; H, 6.84; N, 6.79.

**Triphenyl(4-((4,7,10-tris(carboxymethyl)-1,4,7,10-tetraazacyclododecan-1-yl)methyl)benzyl)arsonium** ( $\text{H}_3\text{L}_2$ ). To a solution of  $\text{DO3A}(\text{OBu-t})_3$  (15.6 mg, 0.03 mmol) and (4-bromomethylbenzyl)triphenylarsonium bromide (52.6 mg, 0.1 mmol) in 3 mL of anhydrous DMF was added triethylamine (0.02 mL, 0.15 mmol). The mixture was stirred overnight at room temperature. Upon removal of volatiles under reduced pressure, the residue was dissolved in 2 mL of concentrated HCl to remove the *tert*-butyl ester groups. After being stirred at room temperature for 10–20 min, volatiles removed under reduced pressure. The residue was dissolved in 4 mL of 50% DMF/water mixture, and product was

**Table 1.** HPLC Retention Time and log  $P$  Values for  $^{64}\text{Cu}$ -L1,  $^{64}\text{Cu}$ -L2,  $^{64}\text{Cu}$ -L3, and  $^{99\text{m}}\text{Tc}$ -Sestamibi

compound	RCP (%)	retention time (min)	log $P$ value
$^{99\text{m}}\text{Tc}$ -Sestamibi	$>98$	16.5	$1.09 \pm 0.15$
$^{64}\text{Cu}$ -L1	$>95$	17.5	$-2.67 \pm 0.21$
$^{64}\text{Cu}$ -L2	$>95$	17.7	$-2.65 \pm 0.02$
$^{64}\text{Cu}$ -L3	$>90$	20.9	$-2.02 \pm 0.01$

**Table 2.** Solution Stability Data for the HPLC Purified  $^{64}\text{Cu}$ -L1 in Saline and in the Presence of EDTA mg/mL in 25 mM Phosphate Buffer, pH = 7.5)

time after HPLC purification, h	RCP (in saline)	RCP (in EDTA solution)
0.5	98	98
1.0	98	98
2.0	98	98
4.0	98	98
6.0	98	98

subjected to HPLC purification. Fractions at  $\sim 16.5$  min were collected and lyophilized to give a white powder. The yield was 14 mg (52%). The HPLC retention time was  $\sim 16.3$  min (Method 1) with the purity  $>98\%$ .  $^1\text{H}$  NMR ( $\text{D}_2\text{O}$ , chemical shift  $\delta$  in ppm relative to TMS): 2.80–3.45 (m, 22H), 3.67 (s, 2H,  $\text{CH}_2$ ), 4.63 (s, 2H,  $\text{AsCH}_2$ ), 6.94 (d, 2H,  $\text{C}_6\text{H}_4$ ), 7.23 (d, 2H,  $\text{C}_6\text{H}_4$ ), 7.37–7.73 (m, 15H,  $\text{C}_6\text{H}_5$ ). ES-MS:  $m/z = 755.8$  for  $[\text{M} + \text{H}]^+$  (calcd 756 for  $[\text{C}_{40}\text{H}_{48}\text{N}_4\text{O}_6\text{As}]^+$ ). Anal. Calcd for  $\text{C}_{42}\text{H}_{51}\text{AsN}_4\text{O}_8\cdot 2.5\text{H}_2\text{O}$ : C, 58.67; H, 6.56; N, 6.52. Found: C, 58.75; H, 6.31; N, 6.68.

**Tris(4-methoxyphenyl)(4-((4,7,10-tris(carboxymethyl)-1,4,7,10-tetraazacyclododecan-1-yl)methyl)benzyl)phosphonium** ( $\text{H}_3\text{L}_3$ ). To a solution of (4-(bromomethyl)benzyl)tris(4-methoxyphenyl)phosphonium bromide (61.9 mg, 0.1 mmol) and  $\text{DO3A}(\text{OBu-t})_3$  (52.0 mg, 0.1 mmol) in 3 mL of anhydrous DMF was added triethylamine (0.07 mL, 0.5 mmol). The reaction mixture was stirred overnight at room temperature. Upon complete removal of DMF and excess triethylamine, the residue was dissolved in 2.2 mL of concentrated HCl (37%). After the mixture was stirred at room temperature for 10–20 min, excess HCl was removed under the reduced pressure. The residue was dissolved in 5 mL of 50% DMF/water mixture, and the product was subjected to semi-prep HPLC purification. Fractions at  $\sim 19$  min were collected. The collected fractions were combined and lyophilized to give a white powder. The yield was 39 mg (48.7%). The HPLC retention time was  $\sim 19.2$  min (Method 1) with the purity  $>98\%$ .  $^1\text{H}$  NMR ( $\text{D}_2\text{O}$ , chemical shift  $\delta$  in ppm relative to TMS): 2.64–3.38 (m, 22H); 3.63 (s, 2H,  $\text{CH}_2$ ); 3.73 (s, 9H,  $\text{CH}_3$ ); 4.35 (d, 2H,  $\text{PCH}_2$ ,  $J_{\text{PH}} = 13$  Hz), 6.67–7.37 (m, 16H,  $\text{C}_6\text{H}_4$ ). ES-MS:  $m/z = 801.4$  for  $[\text{M} + \text{H}]^+$  (calcd 801 for  $[\text{C}_{43}\text{H}_{54}\text{N}_4\text{O}_9\text{P}]^+$ ). Anal. Calcd for  $\text{C}_{45}\text{H}_{57}\text{N}_4\text{O}_{11}\text{P}$ : C, 62.78; H, 6.67; N, 6.51. Found: C, 62.68; H, 7.05; N, 6.60.

**Cu-L1.** To the solution containing  $\text{H}_3\text{L}_1$  (40 mg, 0.56 mmol) and  $\text{Cu}(\text{OAc})_2\cdot 2\text{H}_2\text{O}$  (12.0 mg, 0.60 mmol) in  $\text{H}_2\text{O}$  (2 mL) was added 0.2 mL of  $\text{NH}_4\text{OAc}$  buffer (0.5 M, pH = 6.0). The resulting solution was heated at  $100^\circ\text{C}$  for 45 min. After filtration, diethyl ether (15 mL) was added to the filtrate above. The precipitate was separated and dried under vacuum overnight before being submitted for elemental analysis. The yield was 26.5 mg ( $\sim 61.2\%$ ). A sample was analyzed by HPLC. The HPLC retention time was 17.2 min with the purity  $>95\%$ . IR ( $\text{cm}^{-1}$ , KBr pellet): 1633.5 (s,  $\nu_{\text{C=O}}$ ), 1721.3 (s,  $\nu_{\text{C=O}}$ ) and 3432.1 (bs,  $\nu_{\text{O-H}}$ ). ES-MS (positive mode):  $m/z = 773.3$  for  $[\text{M} + \text{H}]^+$  (calcd 773 for  $[\text{C}_{40}\text{H}_{46}\text{CuN}_4\text{O}_6\text{P}]^+$ ). Anal. Calcd for  $\text{C}_{40}\text{H}_{46}\text{CuN}_4\text{O}_6\cdot 2\text{H}_2\text{O}$ : C, 59.33; H, 6.18; N, 6.92. Found: C, 59.11; H, 6.13; N, 6.63.

**$^{64}\text{Cu}$ -Labeling.** *Caution!*  $^{64}\text{Cu}$  has a half-life of 12.7 h with a  $\beta^+$  emission ( $E_{\text{max}} = 0.655$  MeV, 19.3%), a  $\beta^-$  emission ( $E_{\text{max}} = 0.573$  MeV, 39.6%) and an Auger-electron emission (41%). All manipulations must be performed in a laboratory approved for handling of radioisotopes. Radiation safety procedures must be followed at all times to prevent contamination. To a 5 mL vial

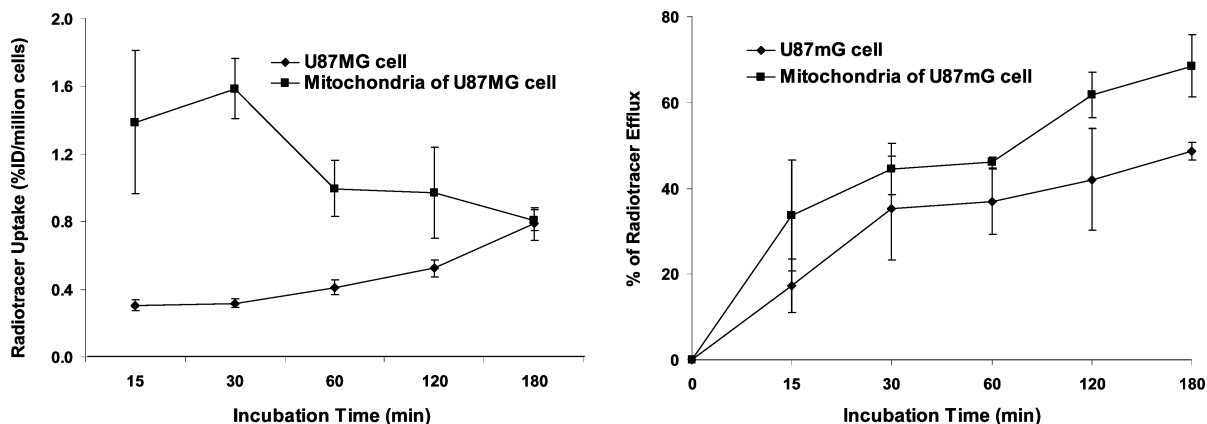


**Figure 3.** Cellular and mitochondrial uptake (left) and efflux (right) kinetics of  $^{64}\text{Cu}$ -L1 in both U87MG human glioma cells (◆) and tumor cell mitochondria (■). The radiotracer uptake is expressed as the percentage of total added radioactivity (%ID). The radiotracer efflux is represented by the percentage of the intracellular radioactivity at  $t = 0$  before being recultured.

were added 0.5 mL of 0.1 M NaOAc buffer (pH = 6.9) containing 50  $\mu\text{g}$  of the DO3A conjugate and 0.12 mL of  $^{64}\text{CuCl}_2$  solution (1.0–2.0 mCi) in 0.05 N HCl. The final pH in the reaction mixture was 5.0–5.5. The mixture was then heated at 100 °C for 30 min. After being cooled to room temperature, a sample of resulting solution was analyzed by radio-HPLC (Method 2). The radiochemical purity (RCP) was >90% for all three radiotracers before purification. The specific activity was 30–50 Ci/mmol for all three  $^{64}\text{Cu}$  radiotracers. The HPLC retention time was ~17.5 min for  $^{64}\text{Cu}$ -L1 and  $^{64}\text{Cu}$ -L2, and 20.4 min for  $^{64}\text{Cu}$ -L3. The HPLC concordance experiment was performed by sequential injection of HPLC-purified  $^{64}\text{Cu}$ -L1 and Cu-L1 under identical chromatographic conditions.

**Dose Preparation.** All three  $^{64}\text{Cu}$  radiotracers were purified by HPLC before being used for biodistribution studies. Volatiles in the HPLC mobile phase were completely removed. The residue was dissolved in saline to give a concentration of ~10  $\mu\text{Ci}/\text{mL}$ . The resulting solution was filtered with a 0.20  $\mu\text{m}$  filter unit to eliminate any particles. Each animal was administered with ~0.10 mL of the dose solution. For the imaging study,  $^{64}\text{Cu}$ -L1 was prepared and the resulting mixture was used without purification. The reaction mixture was diluted to ~5 mCi/mL with saline. The injected dose for each tumor-bearing mouse was about 250  $\mu\text{Ci}$  of  $^{64}\text{Cu}$ -L1.

**Solution Stability.** For solution stability in saline,  $^{64}\text{Cu}$ -L1 was prepared and purified by HPLC. Volatiles in the HPLC mobile phase were removed under vacuum. The residue was dissolved in saline to ~1 mCi/mL. Samples were analyzed by HPLC (Method 2) at 0, 1, 2, 4, and 8 h post purification. In EDTA challenge experiment, the radiotracer was dissolved in 25 mM phosphate buffer (pH = 7.4) containing EDTA (1 mg/mL) to give a concentration of 1 mCi/mL. Samples were analyzed by radio-HPLC (Method 2) at 0, 1, 2, 4, and 8 h post purification.

**Partition Coefficient.** All three radiotracers were purified by HPLC. After complete removal of volatiles in the mobile phase, the residue was dissolved in a mixture of 3 mL of saline and 3 mL of *n*-octanol in a round-bottom flask. The mixture was vigorously stirred for 20 min at room temperature and was then transferred to an Eppendorf microcentrifuge tube. The tube was centrifuged at 12 500 rpm for 5 min. Samples in triplets from *n*-octanol and aqueous layers were obtained and were counted in a gamma-counter (Perkin-Elmer Wizard – 1480). For comparison purposes, the log  $P$  of  $^{99\text{m}}\text{Tc}$ -Sestamibi was also determined using the same procedure. The log  $P$  value was reported as an average of the data obtained in three independent measurements.

**Mitochondria Isolation.** U87MG cells were collected and mitochondria were isolated by Mitochondria Isolation Kit for Cultured Cells (Pierce Biotechnology, Rockford, IL). Briefly, 800  $\mu\text{L}$  of Mitochondria Isolation Reagent A was added to a pellet of  $2 \times 10^7$  U87MG cells. The mixture was vortexed at the medium speed for 5 s and was then incubated on ice for 2 min. After addition

of 10  $\mu\text{L}$  of Mitochondria Isolation Reagent B, the mixture was vortexed at the maximum speed for 5 s and was then incubated on ice for another 5 min. Upon addition of Mitochondria Isolation Reagent C (800  $\mu\text{L}$ ), the mixture was centrifuged at 700g for 10 min at 4 °C. The supernatant was transferred to a new tube and was then centrifuged at 12 000g for 15 min at 4 °C. The supernatant was discarded. To the pellet was added 500  $\mu\text{L}$  of Mitochondria Isolation Reagent C. After centrifugation at 12 000g for 5 min at 4 °C, the mitochondrial pellet was put on ice for the uptake and efflux experiments.

**In Vitro Cellular and Mitochondrial Uptake.** U87MG cells were seeded into 12-well plates ( $8 \times 10^5$  cells/well) overnight. Adherent cells were washed with PBS buffer, followed by addition of  $^{64}\text{Cu}$ -L1 (10  $\mu\text{Ci}$  in 1 mL of DMEM medium per well). After incubation at 37 °C for the specified time (15, 30, 60, 120, and 180 min), cell monolayers were washed with PBS (3 $\times$ ) and then lysed with NaOH–SDS (0.2 N NaOH, 1% SDS). The lysate was counted by a  $\gamma$ -counter (Perkin-Elmer Wizard – 1480). The same procedure was used to carry out the mitochondrial uptake experiment with the mitochondria isolated from the same number of glioma cells.

**Time Dependent Efflux from Cells and Mitochondria.** U87MG cells were seeded into 12-well plates ( $8 \times 10^5$  cells/well) overnight. Adherent cells were washed with PBS, followed by addition of  $^{64}\text{Cu}$ -L1 (10  $\mu\text{Ci}$  in 1 mL of DMEM medium per well). After incubation at 37 °C for 180 min, the medium was removed. The glioma cells were washed with PBS (3 $\times$ ), isolated, and recultured with the radioactivity free DMEM medium for the specified time (0, 15, 30, 60, 120, and 180 min). Cell monolayers were washed with PBS (3 $\times$ ) and were then lysed with NaOH–SDS (0.2 N NaOH, 1% SDS). The lysate was counted by a  $\gamma$ -counter (Perkin-Elmer Wizard – 1480). For the mitochondrial efflux experiment, the mitochondria isolated from the same number of glioma cells were incubated with  $^{64}\text{Cu}$ -L1 in the DMEM medium for 180 min and were then incubated in nonradioactive DMEM medium for the specified time (0, 15, 30, 60, 120, and 180 min). The mitochondrion-bound activity was then isolated from centrifugation after PBS wash (3 $\times$ ) and counted.

**Animal Model.** Biodistribution studies were performed using the athymic nude mice bearing U87MG human glioma xenografts in compliance the NIH animal experiment guidelines (*Principles of Laboratory Animal Care*, NIH Publication No. 86-23, revised 1985). The animal protocol has been approved by Purdue University Animal Care and Use Committee (PACUC). Female athymic nu/nu mice were purchased from Harlan (Charles River, MA) at 4–5 weeks of age. The mice were orthotopically implanted with  $5 \times 10^6$  the U87MG human glioma cells into the mammary fat pad. Tumor cells were grown at 37 °C in Minimal Essential Medium (Alpha Modification) containing 3.7 g of sodium bicarbonate/L, 10% fetal bovine serum v/v, in a humidified atmosphere of 5% carbon dioxide. Four weeks after inoculation, the tumor size was

**Table 3.** Biodistribution Data of  $^{64}\text{Cu}$ -L1 in Athymic Nude Mice Bearing the U87MG Human Glioma Xenografts<sup>a</sup>

organ	uptake (% ID/g)			
	5 min	30 min	60 min	120 min
blood	4.54 ± 0.34	0.91 ± 0.18	1.37 ± 0.67	0.55 ± 0.09
brain	0.18 ± 0.06	0.13 ± 0.17	0.04 ± 0.03	0.05 ± 0.02
heart	2.04 ± 0.35	0.59 ± 0.16	0.84 ± 0.22	0.59 ± 0.02
intestine	13.05 ± 1.52	8.83 ± 9.72	5.54 ± 1.12	2.60 ± 0.24
kidney	21.32 ± 5.44	3.19 ± 0.35	3.29 ± 0.73	2.20 ± 0.42
liver	31.40 ± 4.52	18.73 ± 3.51	15.48 ± 3.53	11.09 ± 2.61
lungs	4.28 ± 0.58	1.72 ± 0.48	1.99 ± 0.64	1.56 ± 0.05
muscle	1.42 ± 0.39	0.10 ± 0.08	0.37 ± 0.37	0.01 ± 0.00
spleen	1.54 ± 0.34	1.06 ± 0.48	0.81 ± 0.19	0.55 ± 0.17
tumor	3.22 ± 0.12	1.61 ± 0.55	2.09 ± 0.82	2.51 ± 0.38
tumor/blood ratio	0.71 ± 0.04	0.71 ± 0.63	2.08 ± 1.86	3.72 ± 1.47
tumor/brain ratio	21.17 ± 10.69	34.66 ± 24.58	119 ± 45	39.72 ± 17.99
tumor/lung	0.79 ± 0.08	0.97 ± 0.42	1.58 ± 0.14	1.66 ± 0.25
tumor/muscle ratio	2.03 ± 0.18	7.36 ± 10.10	137 ± 183	226 ± 50

<sup>a</sup> Each data point represents an average of biodistribution data in four animals.

**Table 4.** Biodistribution Data of  $^{64}\text{Cu}$ -L2 in Athymic Nude Mice Bearing the U87MG Human Glioma Xenografts<sup>a</sup>

organ	uptake (% ID/g)			
	5 min	30 min	60 min	120 min
blood	4.00 ± 0.43	0.67 ± 0.08	0.66 ± 0.27	0.57 ± 0.13
brain	0.19 ± 0.14	0.04 ± 0.00	0.02 ± 0.01	0.05 ± 0.03
heart	1.87 ± 0.66	0.28 ± 0.13	0.37 ± 0.13	0.51 ± 0.22
intestine	13.80 ± 7.28	7.56 ± 3.61	5.17 ± 3.82	2.12 ± 0.88
kidney	14.17 ± 0.77	2.66 ± 0.32	2.48 ± 1.08	2.20 ± 0.49
liver	26.29 ± 0.45	14.83 ± 2.22	12.58 ± 1.55	10.85 ± 2.93
lungs	3.56 ± 1.05	0.96 ± 0.07	1.01 ± 0.53	1.48 ± 0.25
muscle	1.47 ± 0.82	0.03 ± 0.02	0.07 ± 0.11	0.01 ± 0.00
spleen	1.30 ± 0.14	0.46 ± 0.17	0.50 ± 0.36	0.46 ± 0.13
tumor	2.52 ± 0.30	1.25 ± 0.22	1.66 ± 0.64	2.30 ± 1.03
tumor/blood ratio	0.63 ± 0.01	1.87 ± 0.35	2.56 ± 0.58	4.16 ± 2.05
tumor/brain ratio	18.47 ± 9.84	29.98 ± 7.02	114 ± 52.49	69.01 ± 54.86
tumor/lung	0.75 ± 0.23	1.30 ± 0.14	1.72 ± 0.29	1.62 ± 0.36
tumor/muscle ratio	2.31 ± 1.62	27.30 ± 3.09	251 ± 16.57	170 ± 15.70

<sup>a</sup> Each data point represents an average of biodistribution data in four animals.

**Table 5.** Biodistribution Data of  $^{64}\text{Cu}$ -L3 in Athymic Nude Mice Bearing the U87MG Human Glioma Xenografts<sup>a</sup>

organ	uptake (% ID/g)			
	5 min	30 min	60 min	120 min
blood	4.76 ± 1.54	0.48 ± 0.20	0.41 ± 0.21	0.24 ± 0.08
brain	0.13 ± 0.06	0.01 ± 0.00	0.01 ± 0.00	0.01 ± 0.00
heart	2.25 ± 0.75	0.42 ± 0.04	0.32 ± 0.20	0.34 ± 0.10
intestine	7.29 ± 2.15	5.34 ± 3.55	1.97 ± 0.97	1.50 ± 0.15
kidney	18.83 ± 7.53	3.60 ± 0.71	2.63 ± 0.51	1.99 ± 0.23
liver	12.61 ± 1.34	9.69 ± 1.00	6.21 ± 1.45	4.71 ± 0.06
lungs	5.04 ± 0.42	1.02 ± 0.30	0.79 ± 0.12	1.02 ± 0.21
muscle	1.48 ± 0.25	0.11 ± 0.15	0.10 ± 0.16	0.01 ± 0.00
spleen	1.83 ± 0.25	0.36 ± 0.11	0.52 ± 0.09	0.25 ± 0.19
tumor	2.79 ± 0.66	1.47 ± 0.81	1.16 ± 0.20	1.85 ± 0.33
tumor/blood ratio	0.60 ± 0.09	3.03 ± 0.83	3.56 ± 2.11	8.27 ± 2.84
tumor/brain ratio	25.50 ± 17.92	147 ± 81.32	110 ± 10.18	185 ± 32.94
tumor/lungs	0.55 ± 0.12	1.39 ± 0.37	1.49 ± 0.24	1.82 ± 0.21
tumor/muscle ratio	1.88 ± 0.37	46.74 ± 43.14	71.35 ± 57.57	184 ± 32.94

<sup>a</sup> Each data point represents an average of biodistribution data in four animals.

in the range of 0.3–0.6 g, and animals were used for biodistribution and imaging studies.

**Biodistribution Protocol.** Sixteen tumor-bearing mice (20–25 g) were randomly divided into four groups, each of which had four animals. The HPLC-purified  $^{64}\text{Cu}$  radiotracer ( $\sim 1 \mu\text{Ci}$  dissolved in 0.1 mL of saline) was administered each animal via tail vein. Four animals were sacrificed by exsanguinations and opening of thoracic cavity at 5, 30, 60, and 120 min postinjection (p.i.). Organs were excised, washed with saline, dried with absorbent tissue, weighed, and counted on a  $\gamma$ -counter (Perkin-Elmer Wizard – 1480). Organs of interest included tumor, blood, brain, spleen, lungs, liver, kidneys, muscle, and intestine. The organ uptake was calculated as a percentage of the injected dose per gram of wet tissue (%ID/g). For comparison purpose, the biodistribution study

was also performed on  $^{99\text{m}}\text{Tc}$ -Sestamibi, a well-known radiopharmaceutical approved for both myocardial perfusion and tumor imaging, using the same protocol. The biodistribution data and target-to-background ratios are reported as an average plus the standard variation. Comparison between two different radiotracers was also made using the one-way ANOVA test. The level of significance was set at  $p < 0.05$ .

**Metabolism.** The metabolic stability of  $^{64}\text{Cu}$ -L1 was evaluated in normal athymic nude mice. Two animals were anesthetized with IP injection of ketamine (40–100 mg/kg) and xylazine (2–5 mg/kg). Each mouse was administered with  $^{64}\text{Cu}$ -L1 at a dose of 100  $\mu\text{Ci}$  dissolved in 0.2 mL of saline via tail vein. Urine samples were collected at 30 and 120 min p.i. by manual void and were mixed with an equal volume of acetonitrile. The mixture was centrifuged

**Table 6.** Biodistribution Data of  $^{99m}\text{Tc}$ -Sestamibi in Athymic Nude Mice Bearing the U87MG Human Glioma Xenografts<sup>a</sup>

organ	uptake (% ID/g)			
	5 min	30 min	60 min	120 min
blood	0.87 ± 0.48	0.23 ± 0.25	0.07 ± 0.02	0.07 ± 0.03
brain	0.22 ± 0.05	0.14 ± 0.06	0.11 ± 0.02	0.07 ± 0.01
heart	19.22 ± 7.62	17.24 ± 3.84	17.82 ± 3.42	19.19 ± 5.32
intestine	9.80 ± 3.01	10.26 ± 2.70	13.31 ± 3.89	6.19 ± 2.94
kidney	37.45 ± 13.15	28.49 ± 6.00	24.28 ± 4.91	13.50 ± 4.48
liver	14.37 ± 1.01	8.59 ± 1.17	7.29 ± 1.27	4.70 ± 2.31
lungs	6.20 ± 2.59	2.57 ± 0.70	1.81 ± 0.34	1.55 ± 0.54
muscle	4.84 ± 1.22	4.72 ± 1.22	4.83 ± 1.46	5.45 ± 1.24
spleen	3.21 ± 1.39	1.94 ± 0.63	1.51 ± 0.23	1.77 ± 0.90
tumor	3.06 ± 1.15	2.11 ± 0.47	1.47 ± 0.54	1.55 ± 0.36
tumor/blood	6.28 ± 4.44	12.88 ± 2.49	18.55 ± 5.72	23.50 ± 9.83
tumor/brain	16.69 ± 8.72	16.87 ± 7.95	12.53 ± 5.02	22.62 ± 10.34
tumor/lungs	0.69 ± 0.07	0.95 ± 0.34	0.89 ± 0.15	1.22 ± 0.32
tumor/muscle	0.63 ± 0.36	0.46 ± 0.05	0.26 ± 0.10	0.24 ± 0.06

<sup>a</sup> Each data point represents an average of biodistribution data in three animals.

at 8000 rpm. The supernatant was collected and filtered through a 0.20  $\mu\text{m}$  Millex-LG syringe-driven filter unit to remove the precipitate and large proteins. The filtrate was analyzed by radio-HPLC. Feces samples were collected at  $\sim$ 120 min p.i. and were suspended in a mixture of 50% acetonitrile aqueous solution. The mixture was vortexed for 5–10 min. After centrifuging at 8000 rpm for 5 min, the supernatant was collected and passed through a 0.20  $\mu\text{m}$  Millex-LG syringe driven filter unit. The filtrate was then analyzed by radio-HPLC (Method 2).

**Calibration of microPET.** Scanner activity calibration was performed to map between microPET image units and units of activity concentration. A preweighed 50-mL centrifuge tube filled with solution containing  $^{64}\text{CuCl}_2$  ( $\sim$ 9.3 MBq as determined by the dose calibrator) was used to simulate the whole body of the mouse. This tube was weighed, centered in the scanner aperture, and imaged for a 30 min static image. From the sample weight and assuming a density of 1 g/mL, the activity concentration in the bottle was calculated in units of  $\mu\text{Ci/mL}$ . Eight planes were acquired in the coronal section. A rectangular region of interest (ROI) (counts/pixel/ s) was drawn on the middle of eight coronal planes. Using these data, a calibration factor was obtained by dividing the known radioactivity in the cylinder ( $\mu\text{Ci/mL}$ ) by the image ROI. This calibration factor was determined periodically and did not vary significantly with time.

**MicroPET Imaging Studies.** PET imaging of tumor-bearing mice was performed using a microPET R4 rodent model scanner (Concorde Microsystems, Knoxville, TN). The U87MG tumor-bearing mice ( $n = 3$ ) were imaged in the prone position in the microPET scanner. The tumor-bearing mice were injected with  $\sim$ 250  $\mu\text{Ci}$  of  $^{64}\text{Cu-L1}$  via the tail vein and then anesthetized with 2% isoflurane and placed near the center of the FOV where the highest resolution and sensitivity are obtained. Multiple static scans were obtained at 0.05, 0.2, 0.6, 2, and 19 h p.i. The images were reconstructed by a two-dimensional ordered subsets expectation maximum (OSEM) algorithm. No correction was necessary for attenuation or scatter. At each microPET scan, ROIs were drawn over each tumor and major organs on decay-corrected whole-body coronal images. The average radioactivity concentration (accumulation) within the tumor or an organ was obtained from mean pixel values within the multiple ROI volume, which were converted to counts/mL/ min by using the calibration constant C. Assuming a tissue density of 1 g/mL, the ROIs were then converted to counts/g/min and then divided by the total administered activity to obtain an imaging ROI-derived percentage administered activity per gram of tissue (%ID/g).

## Results

**Synthesis of DO3A Conjugates.** We are particularly interested  $\text{H}_3\text{L1}$ ,  $\text{H}_3\text{L2}$ , and  $\text{H}_3\text{L3}$  since they allow us to assess the possible impact of heteroatoms (P versus As) and methoxy groups of the TPP/TPA cations on biodistribution characteristics

of the  $^{64}\text{Cu}$  radiotracers. DO3A is the bifunctional chelator of our choice because it is able to form stable radiometal chelates with many radionuclides, including  $^{64}\text{Cu}$  and  $^{68}\text{Ga}$  for PET,  $^{111}\text{In}$  for SPECT, and  $^{90}\text{Y}$  and  $^{177}\text{Lu}$  for radiotherapy.  $\text{H}_3\text{L1}$ ,  $\text{H}_3\text{L2}$ , and  $\text{H}_3\text{L3}$  were prepared by reacting DO3A(OBu-t)<sub>3</sub> with the corresponding bromide (Chart 1). Hydrolysis of the *tert*-butyl ester with concentrated HCl gave the expected product, which was then subjected to HPLC purification. All three DO3A conjugates were isolated as the monoacetate salt and have been characterized by NMR, ESI-MS, and elemental analysis. The purity of the HPLC-purified DO3A conjugate must be  $>95\%$  before being used for radiolabeling.

**Synthesis and Characterization of Cu-L1.** Cu-L1 is used as a model compound for structural characterization of  $^{64}\text{Cu}$ -labeled TPP/TPA cations. Cu-L1 was prepared by reacting  $\text{H}_3\text{L1}$  with 1 equiv of Cu(II) acetate in 0.5 M ammonium acetate buffer (pH = 6), was isolated as its Zwitterion salt, and has been characterized by IR, ESI-MS, and elemental analysis. The IR spectrum of Cu-L1 shows a broad band at 3432.1  $\text{cm}^{-1}$  from the crystallization water, a strong band at 1721.3  $\text{cm}^{-1}$  from the uncoordinated carboxylate group, and a strong band at 1637.1  $\text{cm}^{-1}$  from two coordinated carboxylate groups. The ESI-MS spectrum of Cu-L1 displays two molecular ions:  $m/z = 773.3$  for  $[\text{M} + \text{H}]^+$  and  $m/z = 795.2$  for  $[\text{M} + \text{Na}]^+$ . Many attempts were made to grow crystals for structural determination of Cu-L1 by X-ray crystallography, but they were unsuccessful. On the basis of its elemental analysis and IR spectroscopic data, we believe that Cu-L1 might exist as its zwitterion form in the solid state as observed for Mn-L1, which has been structurally characterized by X-ray crystallography in our previous study.<sup>44</sup>

**Radiochemistry.** All three  $^{64}\text{Cu}$  radiotracers were prepared by reacting  $^{64}\text{CuCl}_2$  with the DO3A conjugate ( $\text{H}_3\text{L1}$ ,  $\text{H}_3\text{L2}$ , or  $\text{H}_3\text{L3}$ ) in 0.1 M NaOAc buffer (pH = 5.0–5.5) at 100  $^\circ\text{C}$  for 30 min. Their radiochemical purity (RCP) was  $>90\%$  with the specific activity in the range of 30–50 Ci/mmol. Their log  $P$  values (Table 1) were determined to be  $-2.67 \pm 0.21$ ,  $-2.65 \pm 0.02$ , and  $-2.02 \pm 0.01$ , respectively, in the mixture of *n*-octanol and 25 mM phosphate buffer (pH 7.4).  $^{64}\text{Cu-L1}$  is stable for  $>6$  h after purification and remains intact for  $>6$  h without any decomposition (Table 2) in the presence of EDTA (1 mg/mL in 25 mM phosphate buffer, pH = 7.4), which is completely consistent with the metabolic stability of  $^{64}\text{Cu-L1}$  in urine samples of normal mice under anesthesia. We performed the HPLC concordance experiment using HPLC-purified  $^{64}\text{Cu-L1}$  and Cu-L1. Figure 2 shows radio-HPLC chromatograms of  $^{64}\text{Cu-L1}$  and Cu-L1 under the same chromatographic conditions. Since  $^{64}\text{Cu-L1}$  and Cu-L1 have almost identical HPLC retention

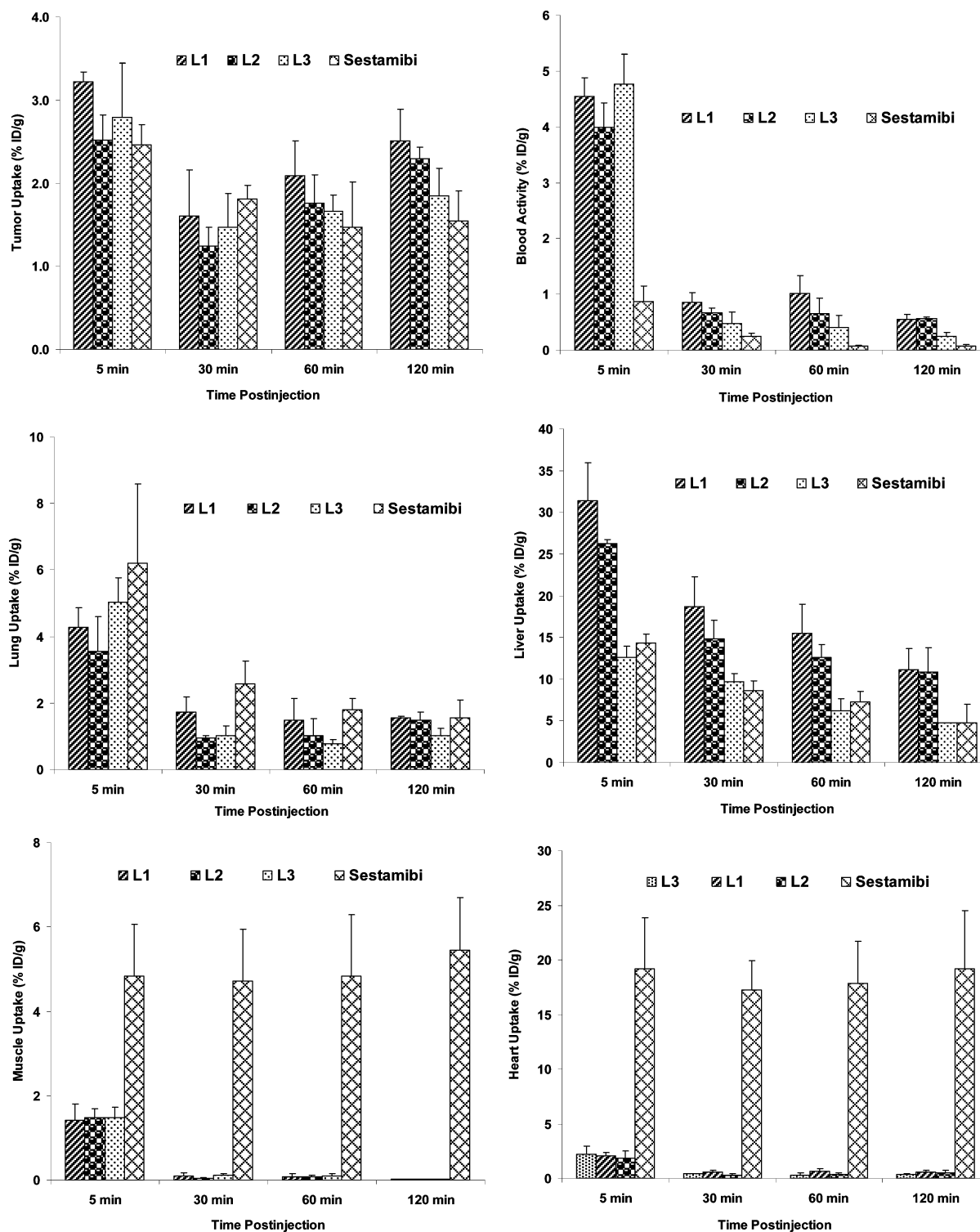


**Figure 4.** Direct comparison of organ uptake (tumor, blood, heart, liver, lungs, and muscle) between  $^{64}\text{Cu}$ -L1,  $^{64}\text{Cu}$ -L2,  $^{64}\text{Cu}$ -L3, and  $^{99\text{m}}\text{Tc}$ -Sestamibi in athymic nude mice bearing U87MG human glioma xenografts. The most striking difference between  $^{64}\text{Cu}$  radiotracers and  $^{99\text{m}}\text{Tc}$ -Sestamibi is uptake in the heart and muscle.

times, it is reasonable to conclude that the same metal complex was prepared at both tracer ( $^{64}\text{Cu}$ ) and macroscopic (Cu) levels. For comparison purposes, we also included the HPLC chromatogram of Mn-L1 under the same chromatographic conditions.<sup>44</sup> It is quite clear that Cu-L1 and Mn-L1 have almost identical HPLC retention times ( $\sim 17.5$  min).

**In vitro Cellular and Mitochondrial Uptake Kinetics.** The cellular and mitochondrial uptake kinetics of  $^{64}\text{Cu}$ -L1 was examined by using U87MG glioma cells. These studies were

designed to demonstrate that  $^{64}\text{Cu}$ -labeled TPP cations are indeed able to cross plasma and mitochondrial membranes and localize in mitochondria of tumor cells. Figure 3 illustrates the cellular and mitochondrial uptake (left) and efflux (right) kinetics of  $^{64}\text{Cu}$ -L1. The radiotracer uptake is expressed as the percentage of total added radioactivity (%ID). The radiotracer efflux is expressed by the percentage of intracellular radioactivity at  $t = 0$  before being recultured. The uptake of  $^{64}\text{Cu}$ -L1 in the tumor cell mitochondria ( $1.39 \pm 0.43$  and  $0.97 \pm 0.27$  %ID/million

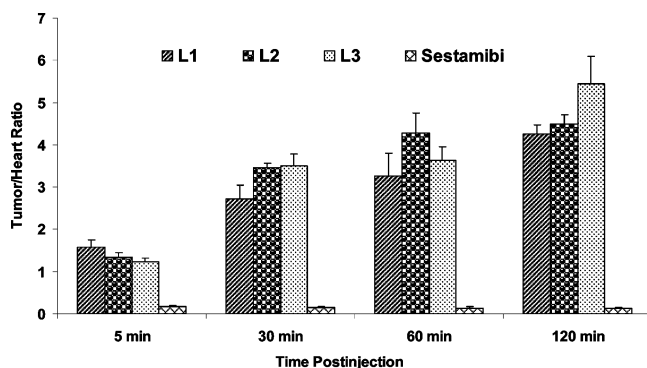


**Figure 5.** Direct comparison of the tumor/heart ratios between  $^{64}\text{Cu}$ -L1,  $^{64}\text{Cu}$ -L2,  $^{64}\text{Cu}$ -L3, and  $^{99\text{m}}\text{Tc}$ -Sestamibi in athymic nude mice bearing U87MG human glioma xenografts. The high tumor selectivity is observed for all three  $^{64}\text{Cu}$  radiotracers as demonstrated by their higher tumor/heart and tumor-lung ratios than those of  $^{99\text{m}}\text{Tc}$ -Sestamibi.

cells) is fast and is significantly higher than that in glioma cells ( $0.31 \pm 0.03$  and  $0.53 \pm 0.05$  %ID/million cells) between 15 and 120 min postincubation (Figure 3: left). This radiotracer uptake difference disappeared at 180 min postincubation. No peak uptake was achieved in the glioma cells after >3 h incubation at  $37^\circ\text{C}$ . In contrast, the efflux kinetics (Figure 3: right) of  $^{64}\text{Cu}$ -L1 from glioma cells was significantly slower than that from tumor cell mitochondria.

**Biodistribution Characteristics.** Biodistribution characteristics of  $^{64}\text{Cu}$ -L1,  $^{64}\text{Cu}$ -L2, and  $^{64}\text{Cu}$ -L3 were evaluated using the athymic nude mice bearing U87MG human glioma xenografts.  $^{99\text{m}}\text{Tc}$ -Sestamibi was evaluated in the same model for comparison purposes. Biodistribution data of  $^{64}\text{Cu}$ -L1,  $^{64}\text{Cu}$ -L2,  $^{64}\text{Cu}$ -L3, and  $^{99\text{m}}\text{Tc}$ -Sestamibi are summarized in Tables 3–6. Figure 4 shows the comparison of organ uptake between  $^{64}\text{Cu}$ -L1,  $^{64}\text{Cu}$ -L2,  $^{64}\text{Cu}$ -L3, and  $^{99\text{m}}\text{Tc}$ -Sestamibi in tumor, blood, heart, liver, lungs, and muscle. Figure 5 illustrates the comparison of tumor/heart ratios between  $^{64}\text{Cu}$ -L1,  $^{64}\text{Cu}$ -L2,  $^{64}\text{Cu}$ -L3, and  $^{99\text{m}}\text{Tc}$ -Sestamibi.

In general, biodistribution properties of  $^{64}\text{Cu}$ -L1 and  $^{64}\text{Cu}$ -L2 are almost identical within the experimental error. Their initial blood activity level was high ( $4.54 \pm 0.34$  and  $4.00 \pm 0.43$  %ID/g, respectively, at 5 min p.i.), but both are able to clear rapidly from blood ( $0.91 \pm 0.18$  and  $0.67 \pm 0.08$  %ID/g, respectively, at 30 min p.i.) via renal and hepatobiliary routes. The high initial blood activity level might contribute to the high uptake of  $^{64}\text{Cu}$ -L1 and  $^{64}\text{Cu}$ -L2 in tumor ( $3.22 \pm 0.12$  and  $2.52 \pm 0.30$  %ID/g), heart ( $2.04 \pm 0.35$  and  $1.87 \pm 0.66$  %ID/g), kidneys ( $21.32 \pm 5.44$  and  $14.17 \pm 0.77$  %ID/g), lungs ( $4.28 \pm 0.58$  and  $3.56 \pm 1.05$  %ID/g), and muscle ( $1.42 \pm 0.39$  and  $1.47 \pm 0.82$  %ID/g) at 5 min p.i. The biodistribution pattern of  $^{64}\text{Cu}$ -L3 is similar to that of  $^{64}\text{Cu}$ -L1, but its blood clearance is faster. The liver uptake of  $^{64}\text{Cu}$ -L3 is significantly lower ( $p < 0.01$ ) than that of  $^{64}\text{Cu}$ -L1 and  $^{64}\text{Cu}$ -L2 at all four time points. Introduction of three methoxy groups seems to reduce liver uptake and increase renal excretion (Tables 3–6). The heart uptake for all three  $^{64}\text{Cu}$  radiotracers was very low (<0.6% ID/g) at >30 min p.i.

We carried out the biodistribution on  $^{99\text{m}}\text{Tc}$ -Sestamibi because it has been widely used to image tumors by SPECT. The most striking difference between  $^{64}\text{Cu}$ -L1,  $^{64}\text{Cu}$ -L2,  $^{64}\text{Cu}$ -L3, and  $^{99\text{m}}\text{Tc}$ -Sestamibi is their uptake in the heart and muscle (Figure 4). For example, the heart uptake was <0.6% ID/g at >30 min p.i. for  $^{64}\text{Cu}$ -L1,  $^{64}\text{Cu}$ -L2, and  $^{64}\text{Cu}$ -L3 while the heart uptake of  $^{99\text{m}}\text{Tc}$ -Sestamibi was  $19.22 \pm 7.62$  at 5 min p.i. and  $19.19 \pm 5.32$  %ID/g at 120 min p.i. The tumor/heart ratios of  $^{64}\text{Cu}$ -L1,

$^{64}\text{Cu}$ -L2, and  $^{64}\text{Cu}$ -L3 increased steadily from  $\sim 1$  at 5 min p.i. to  $\sim 5$  at 120 min p.i. The tumor/heart ratio of  $^{64}\text{Cu}$ -L3 was about 40-fold better than that of  $^{99\text{m}}\text{Tc}$ -Sestamibi at 120 min p.i. (Figure 5). The muscle uptake for  $^{64}\text{Cu}$ -L1,  $^{64}\text{Cu}$ -L2, and  $^{64}\text{Cu}$ -L3 was almost undetectable at >30 min p.i. In contrast,  $^{99\text{m}}\text{Tc}$ -Sestamibi has a very high muscle uptake ( $4.84 \pm 1.22$  at 5 min p.i. and  $5.45 \pm 1.24$  %ID/g at 120 min p.i.). In addition, the lung uptake of  $^{99\text{m}}\text{Tc}$ -Sestamibi is significantly higher ( $p < 0.05$ ) than that of  $^{64}\text{Cu}$ -L1,  $^{64}\text{Cu}$ -L2, and  $^{64}\text{Cu}$ -L3 at 5–60 min p.i., but this difference disappeared at 2 h p.i.

**PET Imaging.** We performed a MicroPET imaging study on  $^{64}\text{Cu}$ -L1 using athymic nude mice ( $n = 3$ ) bearing U87MG human glioma xenografts. Figure 6 illustrates the coronal microPET images (A) and the activity accumulation quantification (B) in several organs of the tumor-bearing mice administered with  $\sim 250$  mCi of  $^{64}\text{Cu}$ -L1. The glioma tumor was clearly visualized as early as 30 min p.i. with very high tumor-to-background contrast. No significant radioactivity accumulation was detected in the brain. The radioactivity accumulation in the heart and muscle was also very low, which is consistent with the results from ex vivo biodistribution studies. After normalization, the tumor uptake of  $^{64}\text{Cu}$ -L1 is  $1.94 \pm 0.82$  %ID/g,  $2.31 \pm 0.90$  %ID/g,  $2.57 \pm 0.41$  %ID/g,  $3.51 \pm 1.20$  %ID/g, and  $3.11 \pm 1.44$  %ID/g at 3 min, 12 min, 35 min, 2 and 19 h p.i., respectively. The steady increase in tumor uptake between 0.5 and 2 h p.i. is completely consistent with that observed in the biodistribution study (Figure 4), and is supported by the slow “diffusion kinetics” of  $^{64}\text{Cu}$ -L1 in both glioma cells and mitochondria of glioma cells (Figure 3).

**Metabolic Properties.** We performed metabolism studies on  $^{64}\text{Cu}$ -L1 using normal athymic nude mice. Each mouse was administered with  $\sim 100$   $\mu\text{Ci}$  of  $^{64}\text{Cu}$ -L1. Since  $^{64}\text{Cu}$ -L1 is excreted from both renal and hepatobiliary routes, we tried to collect urine and feces samples from the mice administered with  $^{64}\text{Cu}$ -L1. The radio-HPLC was used for sample analysis to determine if  $^{64}\text{Cu}$ -L1 is able to retain its chemical integrity at 2 h p.i. Attempts to collect the urine sample at 120 min p.i. were not successful. Figure 7 illustrates the representative radio-HPLC chromatograms of  $^{64}\text{Cu}$ -L1 (HPLC purified) in saline before injection (A), in the urine sample at 30 min p.i. (B), and in the feces sample at 120 min p.i. (C). There is no significant metabolite detectable in the urine sample at 30 min p.i. while only about 15% of  $^{64}\text{Cu}$ -L1 remains intact in the feces sample at 120 min p.i. The identity of metabolite from the feces sample is not known. Since the species at  $\sim 4$  min is very hydrophilic, it is reasonable to believe that the TPP moiety of  $^{64}\text{Cu}$ -L1 is probably cleaved in the metabolite.

## Discussion

In this study, we reported the synthesis and evaluation of three  $^{64}\text{Cu}$ -labeled TPP cations as PET radiotracers for imaging tumors with much higher mitochondrial potentials than normal cells. Cu-L1 was prepared as a model compound for structural characterization of  $^{64}\text{Cu}$ -labeled TPP/TPA cations. On the basis of its spectroscopic and HPLC data, we believe that Cu-L1 most likely exists in its zwitterion form as observed for Mn-L1.<sup>44</sup> The exact structure of Cu-L1 remains unknown. Since the ionic radius of Cu(II) ( $0.67 \text{ \AA}$ )<sup>45</sup> is very close to that of Ga(III) ( $0.62 \text{ \AA}$ ),<sup>45</sup> the coordinated DO3A in Cu-L1 might be the same as that in  $[\text{Ga-L1}]^+$ ,<sup>44</sup> with one acetate group remaining deprotonated to balance to cationic charge of the TPP moiety.

$^{99\text{m}}\text{Tc}$ -Sestamibi and  $^{99\text{m}}\text{Tc}$ -Tetrofosmin have been widely used for both myocardial perfusion imaging and diagnosis of tumors in clinics.<sup>46–52</sup> However, their cancer diagnostic value

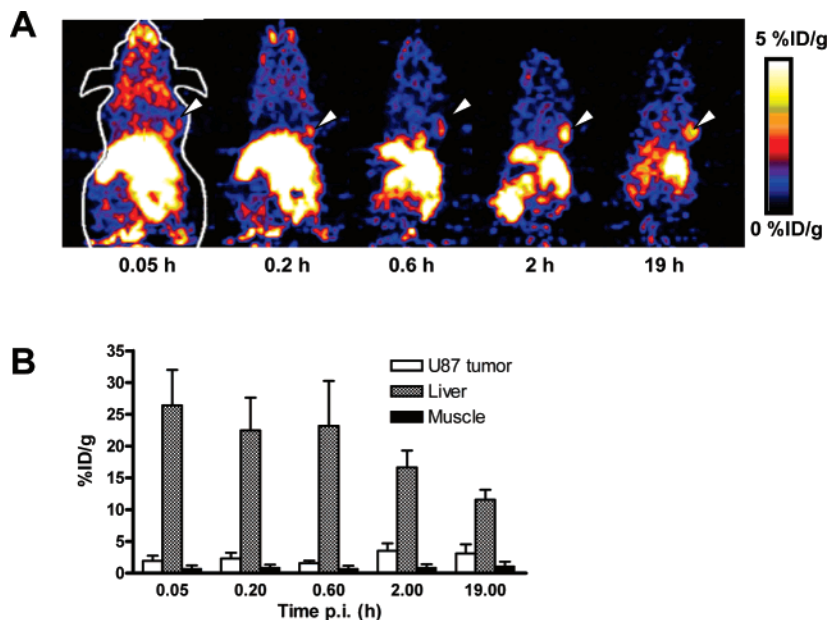


**Figure 6.** The coronal microPET images (top) and the radioactivity accumulation quantification (bottom) in selected organs of the tumor-bearing mice administered with  $\sim 250$  mCi of  $^{64}\text{Cu-L1}$ . Arrows indicate the presence of glioma tumors. All microPET images were decay-corrected.

is often limited because of its insufficient tumor localization and high liver uptake, which makes it very difficult to detect small lesions in the chest and abdominal regions. Radiolabeled lipophilic cations, such as  $^3\text{H-TPP}$  and  $^{18}\text{F-BzTPP}$ , have also been evaluated as radiotracers for imaging heart and tumors.<sup>29–37</sup>  $^3\text{H-TPP}$  has better tumor uptake than  $^{99\text{m}}\text{Tc-Sestamibi}$ , but its tumor selectivity is poor with the tumor/heart ratio  $< 0.2$ . In addition, there is always a high muscle uptake for both  $^3\text{H-TPP}$  and  $^{99\text{m}}\text{Tc-Sestamibi}$ .<sup>31,35</sup>

In this study, we discovered a new class of radiotracers with very high tumor selectivity. All three  $^{64}\text{Cu}$ -labeled TPP cations show the tumor uptake comparable to or better than that of  $^{99\text{m}}\text{Tc-Sestamibi}$  (Figure 4), but their heart uptake is much lower and their tumor/heart ratios are significantly better than those of  $^{99\text{m}}\text{Tc-Sestamibi}$  at all four time points (Figure 5). For example, the tumor/heart ratio of  $^{64}\text{Cu-L1}$  is  $1.57 \pm 0.18$  at 5 min p.i. and increases to  $4.25 \pm 0.23$  at 120 min p.i. while the tumor/heart ratio of  $^{99\text{m}}\text{Tc-Sestamibi}$  is  $< 0.2$  during the 2 h study period. The heart uptake for  $^{64}\text{Cu-L1}$ ,  $^{64}\text{Cu-L2}$ , and  $^{64}\text{Cu-L3}$  is also significantly lower than that of  $^3\text{H-TPP}$  in the same animal species,<sup>35,36</sup> most likely because of high hydrophilicity of the  $^{64}\text{Cu-DO3A}$  chelate. The tumor selectivity of  $^{64}\text{Cu-L1}$ ,  $^{64}\text{Cu-L2}$ , and  $^{64}\text{Cu-L3}$  is unprecedented among all cationic radiotracers reported in the literature,<sup>35,36</sup> including  $^{99\text{m}}\text{Tc-Sestamibi}$  and  $^3\text{H-TPP}$ . Results from the in vitro cellular and mitochondrial uptake experiments (Figure 3) clearly demonstrate that  $^{64}\text{Cu}$ -labeled TPP cations are able to cross the plasma and mitochondrial membranes and localize in mitochondria of tumor cells.

There are several factors affecting the tumor uptake and tumor selectivity of a cationic radiotracer. These include mitochondrial population, mitochondrial potential, and lipophilicity of the radiotracer. Various tumor cell lines exhibit differences in the number, size, and shape of their mitochondria relative to normal cells.<sup>3</sup> The mitochondria of rapidly growing tumors tend to be fewer in number and have fewer cristae than mitochondria from slowly growing tumors; the latter are larger and have characteristics more closely resembling those of normal cells.<sup>3</sup> Thus, the high tumor uptake (2–3 %ID/g) of  $^{64}\text{Cu-L1}$ ,  $^{64}\text{Cu-L2}$ ,  $^{64}\text{Cu-L3}$ , and  $^{99\text{m}}\text{Tc-Sestamibi}$  is not likely related to mitochondrial population in tumor cells. In contrast, the enhanced mitochondrial potential is prevalent in tumor cell phenotype.

The difference in mitochondrial potential between carcinoma cells and normal epithelial cells is  $\sim 60$  mV.<sup>1–4,15</sup> Thus, the enhanced mitochondrial transmembrane potential in tumor cells is most likely responsible for the tumor localization of  $^{64}\text{Cu-L1}$ ,  $^{64}\text{Cu-L2}$ ,  $^{64}\text{Cu-L3}$ , and  $^{99\text{m}}\text{Tc-Sestamibi}$ .

The difference between myocardium and normal tissue is their mitochondrial population. Myocardium has the highest population of mitochondria, which occupy 20–25% of the total volume of myocytes.<sup>31</sup> Other mitochondrion-rich organs also include salivary gland, liver and kidneys. Mechanism studies on  $^{99\text{m}}\text{Tc-Sestamibi}$  indicate that both the lipophilicity and cationic charge play an important role in the accumulation and retention of cationic  $^{99\text{m}}\text{Tc}$  radiotracers in tumor cells and myocytes.<sup>53–55</sup> While the mitochondrial potential provides electrochemical driving force for the radiolabeled lipophilic cations to enter mitochondria of tumor cells, the lipophilicity modulates their penetration kinetics into plasma and mitochondrial membranes. For more lipophilic cationic radiotracers, such as  $^{99\text{m}}\text{Tc-Sestamibi}$  ( $\log P = 1.09 \pm 0.15$ ), their diffusion kinetics are so fast that they tend to localize in the mitochondrion-rich organs, such as heart, liver, kidneys, and salivary gland.<sup>56–59</sup> For more hydrophilic cations, such as  $^{64}\text{Cu-L1}$  ( $\log P = -2.67 \pm 0.21$ ), their membrane diffusion kinetics is very slow (Figure 3: left), which makes it difficult for the more hydrophilic cations across plasma and mitochondrial membranes, thereby forcing them to localize in tissues where the mitochondrial transmembrane potential is elevated. Therefore, it is not surprising that all three  $^{64}\text{Cu}$  radiotracers ( $\log P = -2.03$  to  $-2.67$ ) have low uptake in the heart and muscle with very high tumor/heart selectivity while lipophilic cations, such as  $^{99\text{m}}\text{Tc-Sestamibi}$  and  $^3\text{H-TPP}$ , are excellent myocardial perfusion radiotracers because of the high heart and muscle uptake and long myocardial retention. In this respect, myocardial perfusion radiotracers with very high lipophilicity ( $\log P \approx 0.5–1.3$ ) are particularly useful for imaging “mitochondrial population” while radiotracers with low lipophilicity ( $\log P = 0$  to  $-3.0$ ) are useful for imaging “the enhanced mitochondrial potential”. This conclusion is consistent with the high tumor selectivity of rhodamine-123 ( $\log P = -0.62$ ) and MKT-077 (1-ethyl-2- $\{$ -[3-ethyl-5-(3-methylbenzothiazolin-2-ylidene)]-4-oxothiazolin-2-ylidene $\}$ pyridinium chloride), an anticancer drug with the

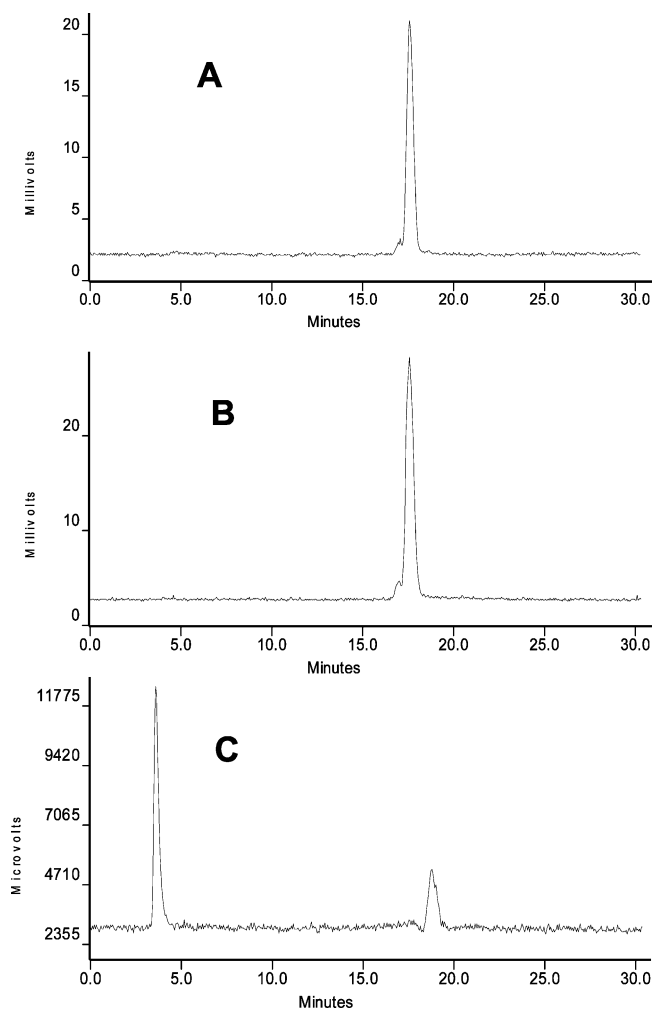


**Figure 7.** Radio-HPLC chromatograms of the HPLC purified  $^{64}\text{Cu}$ -L1 in saline before injection (A), in the urine sample at 30 min postinjection (B), and in the feces sample at 120 min p.i. (C). Attempts to collect the urine sample at 120 min p.i. were not successful. Each mouse was administered with  $\sim 100 \mu\text{Ci}$  of  $^{64}\text{Cu}$ -L1.

$\log P$  value of  $-1.6$ .<sup>60,61</sup> It is also supported by the results obtained from studies on cationic triarylmethane dyes.<sup>62–65</sup>

It is interesting to note that all three  $^{64}\text{Cu}$  radiotracers ( $^{64}\text{Cu}$ -L1,  $^{64}\text{Cu}$ -L2, and  $^{64}\text{Cu}$ -L3) show a sharp decrease in their tumor uptake between 5 and 30 min p.i., and a steady increase in their tumor uptake between 30 and 120 min p.i. while  $^{99\text{m}}\text{Tc}$ -Sestamibi has a slow washout during the 2 h study period (Figure 4). We believe that the high initial tumor uptake of these radiotracers is likely caused by their high blood radioactivity level. The steady increase in tumor uptake suggests that it may take time for radiotracer to form the equilibrium inside/outside tumor cells. The fact that all three  $^{64}\text{Cu}$  radiotracers have a steady increase in their tumor uptake suggests that they are indeed able to localize inside mitochondria, instead of being the “blood-flow” radiotracers. If they were simple blood flow radiotracers, there would have been a significant washout over time due to their rapid blood clearance.

In order to understand the biodistribution properties of  $^{64}\text{Cu}$ -L1,  $^{64}\text{Cu}$ -L2, and  $^{64}\text{Cu}$ -L3, we performed cellular and mitochondrial uptake experiments using  $^{64}\text{Cu}$ -L1 in U87MG glioma cells. It was found that there is a steady increase in cellular uptake of  $^{64}\text{Cu}$ -L1 over 3 h (Figure 3: left). No peak uptake is observed after  $>3$  h incubation at  $37^\circ\text{C}$ . In contrast,  $^{99\text{m}}\text{Tc}$ -Sestamibi shows the cellular uptake plateau in  $<60$  min in several MDR-negative tumor cell lines,<sup>66–68</sup> including human

epithelial carcinoma KB-3-1 cells and HT29<sup>par</sup> colon carcinoma cells. The slow cellular and mitochondrial uptake kinetics is consistent with the observation of a steady increase in the tumor uptake of all three radiotracers ( $^{64}\text{Cu}$ -L1,  $^{64}\text{Cu}$ -L2, and  $^{64}\text{Cu}$ -L3) between 30 and 120 min p.i. in the biodistribution study. The fact that the uptake of  $^{64}\text{Cu}$ -L1 ( $0.31 \pm 0.03$  to  $0.53 \pm 0.05$  %ID/million cells) in glioma cells between 15–120 min postincubation is significantly ( $p < 0.01$ ) lower than that in mitochondria ( $1.39 \pm 0.43$  to  $0.97 \pm 0.27$  %ID/million cells) isolated from glioma cells strongly suggests that the diffusion process across the plasma membrane is a key step for the radiotracer to enter mitochondria of tumor cells. This conclusion is also supported by the slower efflux kinetics of  $^{64}\text{Cu}$ -L1 from glioma cells (Figure 3: right). It must be emphasized that these in vitro data serve only as complimentary evidence, and should not be viewed as “absolute” proof for the in vivo behavior of the radiotracer.

Lipophilicity of a cationic radiotracer has a significant impact on its diffusion kinetics to penetrate both plasma and mitochondrial membranes. For more lipophilic radiotracers, such as  $^{99\text{m}}\text{Tc}$ -Sestamibi ( $\log P = 1.09 \pm 0.15$ ), their membrane diffusion kinetics are fast and they can localize in tumor quickly. For more hydrophilic cations, such as  $^{64}\text{Cu}$ -L1 ( $\log P = -2.67 \pm 0.21$ ), their membrane penetration kinetics is very slow and it takes them several hours to reach the maximal uptake in glioma tumor cells. This explanation is consistent with the slow cellular uptake kinetics of  $^{64}\text{Cu}$ -L1 (Figure 3: left) and is also supported by the fact that  $^{64}\text{Cu}$ -L1 reaches its peak tumor uptake at  $\sim 6$  h p.i. as observed in PET images of tumor-bearing mice (Figure 5). Results from studies of cationic organic dyes also showed that very hydrophilic and water-soluble organic cations ( $\log P < -1.5$ ) will not be reach the equilibrium after 24 h incubation with tumor cells.<sup>63,65</sup>

MDR gene (particularly *MDR1*) expression is another important factor that influences the tumor uptake of cationic radiotracers. In this study, we choose the U87MG glioma cell line since it has very limited *MDR1* expression.<sup>42,43</sup> High *MDR1* expression is expected to result in a rapid efflux of cationic radiotracer from tumor cells and significant reduction of its tumor uptake.<sup>22–25</sup> Thus, the tumor uptake data reported herein reflects the intrinsic capability of  $^{64}\text{Cu}$ -L1,  $^{64}\text{Cu}$ -L2, and  $^{64}\text{Cu}$ -L3 to localize in tumors due to the enhanced mitochondrial potential. It is well-documented that cationic  $^{99\text{m}}\text{Tc}$  radiotracers, such as  $^{99\text{m}}\text{Tc}$ -Sestamibi and  $^{99\text{m}}\text{Tc}$ -Tetrofosmin originally approved as myocardial perfusion radiopharmaceuticals, are clinically useful for noninvasive imaging of the *MDR1* expression in tumors.<sup>17–25</sup> From this point of view,  $^{64}\text{Cu}$ -L1,  $^{64}\text{Cu}$ -L2, and  $^{64}\text{Cu}$ -L3 might be useful for noninvasive imaging of the *MDR* function in different tumors. Biodistribution and imaging studies in tumor-bearing mice with and without *MDR1* expression are still in progress, and the results will be reported as a separate account.

In addition to diagnostic applications, both  $^{64}\text{Cu}$  and  $^{67}\text{Cu}$  are useful for radiotherapy.<sup>39–41</sup>  $^{64}\text{Cu}$  has a low-energy  $\beta$ -emission ( $E_{\text{max}} = 0.573$  MeV, 39.6%) and an Auger-electron emission (41%).  $^{67}\text{Cu}$  has three low-energy  $\beta$ -emissions ( $E_{\text{max}} = 0.577$  MeV, 20%;  $0.484$  MeV, 35%; and  $0.395$  MeV, 45%). DO3A is useful for chelation of various therapeutic radionuclides, such as  $^{111}\text{In}$  (Auger-electron emission),  $^{90}\text{Y}$  (pure  $\beta$ -emission,  $E_{\text{max}} = 2.28$  MeV), and  $^{177}\text{Lu}$  (low-energy  $\beta$ -emission  $E_{\text{max}} = 0.497$  MeV). The fact that  $^{64}\text{Cu}$ -labeled TPP/TPA cations are able to localize in the energized mitochondria of tumor cells suggest that the TPP cations chelated with a low-energy  $\beta$ -particle or an Auger-electron radionuclide might be

very attractive radiotracers for tumor radiotherapy because they will have more opportunities to interact intracellular biomolecules, such as DNA molecules, than the extracellular receptor-based radiotracers. They may also produce more "intracellular" free radicals, which are very reactive toward many biomolecules inside mitochondria of tumor cells. However, in the absence of experimental data, these assumptions remain largely speculation.

## Conclusion

In this study, we discovered a new class of PET radiotracers with very high tumor selectivity. Results from the in vitro cellular and mitochondrial uptake kinetics clearly demonstrate that the  $^{64}\text{Cu}$ -labeled TPP cations are able to across the plasma and mitochondrial membranes and localize in mitochondria of tumor cells. The most striking difference between  $^{64}\text{Cu}$ -L1,  $^{64}\text{Cu}$ -L2,  $^{64}\text{Cu}$ -L3 and  $^{99\text{m}}\text{Tc}$ -Sestamibi is their tumor/heart and heart/muscle ratios. The heart uptake for  $^{64}\text{Cu}$ -L1,  $^{64}\text{Cu}$ -L2, and  $^{64}\text{Cu}$ -L3 is much lower than that of  $^{99\text{m}}\text{Tc}$ -Sestamibi in the same animal model. The tumor selectivity of  $^{64}\text{Cu}$ -L1,  $^{64}\text{Cu}$ -L2, and  $^{64}\text{Cu}$ -L3 is unprecedented among all the cationic radiotracers reported in literature. While their high tumor uptake is due to the enhanced negative mitochondrial transmembrane potentials in glioma cells, their unprecedented high tumor selectivity is attributed to their low lipophilicity ( $\log P = -2.03$  to  $-2.67$ ). The results from this study strongly suggest that the  $^{64}\text{Cu}$ -labeled TPP/TPA cations are very selective tumor-imaging radiotracers, and can provide the information of mitochondrial bioenergetic function by monitoring mitochondrial potential in tumors.

**Acknowledgment.** Authors would like to thank Dr. Sulma I. Muhammed, the Director of Purdue Cancer Center Drug Discovery Shared Resource, Purdue University, for her assistance with the tumor-bearing animal model. This work is supported, in part, by research grants: R01 CA115883 A2 (S.L.) from National Cancer Institute (NCI), BCTR0503947 (S.L.) from Susan G. Komen Breast Cancer Foundation, AHA0555659Z (S.L.) from the Greater Midwest Affiliate of American Heart Association, R21 EB003419-02 (S.L.) from National Institute of Biomedical Imaging and Bioengineering (NIBIB), and R21 HL083961-01 from National Heart, Lung, and Blood Institute (NHLBI).

## References

- Kroemer, G.; Dallaporta, B.; Resche-Rigon, M. The mitochondrial death/ life regulator in apoptosis and necrosis. *Annu. Rev. Physiol.* **1998**, *60*, 619–642.
- Modica-Napolitano, J. S.; Aprille, J. R. Delocalized lipophilic cations selectively target the mitochondria of carcinoma cells. *Adv. Drug Delivery Rev.* **2001**, *49*, 63–70.
- Duchen, M. R. Mitochondria in health and disease: perspectives on a new mitochondrial biology. *Mol. Aspects Med.* **2004**, *25*, 365–451.
- Modica-Napolitano, J. S.; Singh, K. K. Mitochondria as targets for detection and treatment of cancer. *Expert Reviews in Molecular Medicine*. <http://www.ermm.cbuc.cam.ac.uk>, 2002, (02)00445-3a (short code: txt001ksb).
- Johnson, L. V.; Walsh, M. L.; Chen, L. B. Localization of mitochondria in living cells with rhodamine 123. *Proc. Natl. Acad. Sci. U.S.A.* **1980**, *77*, 990–994.
- Summerhayes, I. C.; Lampidis, T. J.; Bernal, S. D.; Nadakavukaren, J. J.; Nadakavukaren, K. K.; Shepard, E. L.; Chen, L. B. Unusual retention of rhodamine 123 by mitochondria in muscle and carcinoma cells. *Proc. Natl. Acad. Sci. U.S.A.* **1982**, *79*, 5292–5296.
- Modica-Napolitano, J. S.; Aprille, J. R. Basis for the selective cytotoxicity of rhodamine 123. *Cancer Res.* **1987**, *47*, 4361–4365.
- Davis, S.; Weiss, M. J.; Wong, J. R.; Lampidis, T. J.; Chen, L. B. Mitochondrial and plasma membrane potentials cause unusual accumulation and retention of rhodamine 123 by human breast adenocarcinoma-derived MCF-7 cells. *J. Biol. Chem.* **1985**, *260*, 3844–3850.
- Dairkee, S. H.; Hackett, A. J. Differential retention of rhodamine 123 by breast carcinoma and normal human mammary tissue. *Breast Cancer Res. Treat.* **1991**, *18*, 57–61.
- Gottlieb, E.; Thompson, C. B. Targeting the mitochondria to enhance tumor suppression. *Methods Mol. Biol.* **2003**, *223*, 543–554.
- Mannella, C. A. The relevance of mitochondrial membrane topology to mitochondrial function. *Biochim. Biophys. Acta* **2006**, *1762*, 140–147.
- Ross, M. F.; Kelso, G. F.; Blaikie, F. H.; James, A. M.; Cocheme, H. M.; Filipovska, A.; Da Ros, T. D.; Hurd, T. R.; Smith, R. A. J.; Murphy, M. P. Lipophilic triphenylphosphonium cations as tools in mitochondrial bioenergetics and free radical biology. *Biochemistry (Moscow)* **2005**, *70*, 222–230.
- Jakobs, S. High resolution imaging of live mitochondria. *Biochim. Biophys. Acta* **2006**, *1763*, 561–575.
- Lichtshtein, D.; Kaback, H. R.; Blume, A. J. Use of a lipophilic cation for determination of membrane potential in neuroblastomas-glioma hybrid cell suspensions. *Proc. Natl. Acad. Sci. U.S.A.* **1979**, *76*, 650–654.
- Hockings, P. D.; Rogers, P. J. The measurement of transmembrane electric potential with lipophilic cations. *Biochim. Biophys. Acta* **1996**, *1282*, 101–106.
- Huang, S. G. Development of a high throughput screening assay for mitochondrial membrane potential in living cells. *J. Biomol. Screening* **2002**, *7*, 383–389.
- Herman, L. W.; Sharma, V.; Kronauge, J. F.; Barbarics, E.; Herman, L. A.; Piwnica-Worms, D. Novel hexakis(areneisonitrile)technetium-(I) complexes as radioligands targeted to the multidrug resistance P-glycoprotein. *J. Med. Chem.* **1995**, *38*, 2955–2963.
- Agrawal, M.; Abraham, J.; Balis, F. M.; Edgerly, M.; Stein, W. D.; Bates, S.; Fojo, T.; Chen, C. C. Increased  $^{99\text{m}}\text{Tc}$ -Sestamibi accumulation in normal liver and drug resistant-tumors after the administration of the glycoprotein inhibitor, XR9576. *Clin. Cancer Res.* **2003**, *9*, 650–656.
- Luker, G. D.; Francisco, P. M.; Dobkin, J.; Piwnica-Worms, D. Modulation of the multidrug resistance P-glycoprotein: Detection with technetium-99m sestamibi in vivo. *J. Nucl. Med.* **1997**, *38*, 369–372.
- Liu, Z. L.; Stevenson, G. D.; Barrett, H. H.; Kastis, G. A.; Bettan, M.; Furenlid, L. R.; Wilson, D. W.; Woolfenden, J. M. Imaging recognition of multidrug resistance in human breast tumors using  $^{99\text{m}}\text{Tc}$ -labeled monocationic agents and a high-resolution stationary SPECT system. *Nucl. Med. Biol.* **2004**, *31*, 53–65.
- Liu, Z. L.; Stevenson, G. D.; Barrett, H. H.; Furenlid, L. R.; Wilson, D. W.; Kastis, G. A.; Bettan, M.; Woolfenden, J. M. Imaging recognition of inhibition of multidrug resistance in human breast cancer xenografts using  $^{99\text{m}}\text{Tc}$ -labeled sestamibi and tetrafosmin. *Nucl. Med. Biol.* **2005**, *32*, 573–583.
- Sharma, V.; Piwnica-Worms, D. Metal complexes for therapy and diagnosis of drug resistance. *Chem. Rev.* **1999**, *99*, 2545–2560.
- Muzzammil, T.; Ballinger, J. R.; Moore, M. J.  $^{99\text{m}}\text{Tc}$ -sestamibi imaging of inhibition of the multidrug resistance transporter in a mouse xenograft model of human breast cancer. *Nucl. Med. Commun.* **1999**, *20*, 115–122.
- Sharma, V. Radiopharmaceuticals for assessment of multidrug resistance P-glycoprotein-mediated drug transport activity. *Bioconjugate Chem.* **2004**, *15*, 1464–1474.
- Vaidyanathan, G.; Zalutsky, M. R. Imaging drug resistance with radiolabeled molecules. *Curr. Pharm. Des.* **2004**, *10*, 2965–2979.
- Woo, D. V. Process of radioimaging the myocardium of mammals utilizing radiolabeled lipophilic cations. US Patent 4,446,123, 1984.
- Srivastava, P. C.; Knapp, F. K. [(E)-1-[ $^{123}\text{I}$ ]iodo-penten-5-yl]triphenylphosphonium iodide: convenient preparation of a potentially useful myocardial perfusion agent. *J. Med. Chem.* **1984**, *27*, 978–981.
- Srivastava, P. C.; Hay, H. G.; Knapp, F. K. Effects of alkyl and aryl substitution on the myocardial specificity of radioiodinated phosphonium, arsinium, and ammonium cations. *J. Med. Chem.* **1985**, *28*, 901–904.
- Krause, B. J.; Szabo, Z.; Becker, L. C.; Dannals, R. F.; Scheffel, U.; Seki, C.; Ravert, H. T.; Dipaola, A. F., Jr.; Wagner, H. N., Jr. Myocardial perfusion with [ $^{11}\text{C}$ ] triphenyl phosphonium: measurements of the extraction fraction and myocardial uptake. *J. Nucl. Biol. Med.* **1994**, *38*, 521–526.
- Madar, I.; Anderson, J. H.; Szabo, Z.; Scheffel, U.; Kao, P. F.; Ravert, H. T.; Dannals, R. F. Enhanced uptake of [ $^{11}\text{C}$ ]TPMP in canine brain tumor: a PET study. *J. Nucl. Med.* **1999**, *40*, 1180–1185.
- Madar, I.; Weiss, L.; Izbicki, G. Preferential accumulation of  $^3\text{H}$ -tetraphenylphosphonium in non-small cell lung carcinoma in mice: comparison with  $^{99\text{m}}\text{Tc}$ -MIBI. *J. Nucl. Med.* **2002**, *43*, 234–238.
- Ravert, H. T.; Madar, I.; Dannals, R. F. Radiosynthesis 3-[ $^{18}\text{F}$ ]fluoropropyl and 4-[ $^{18}\text{F}$ ]fluorobenzyl triarylphosphonium ions. *J. Labelled Compd. Radiopharm.* **2004**, *47*, 469–476.

- (33) Madar, I.; Ravert, H. T.; Du, Y.; Hilton, J.; Volokh, L.; Dannals, R. F.; Frost, J. J.; Hare, J. M. Characterization of uptake of the new PET imaging compound [<sup>18</sup>F]fluorobenzyl triphenylphosphonium in dog myocardium. *J. Nucl. Med.* **2006**, *47*, 1359–1366.
- (34) Cheng, Z.; Subbarayan, M.; Chen, X.; Gambhir, S. S. Synthesis of (4-[<sup>18</sup>F]fluorophenyl)triphenylphosphonium as a potential imaging agent for mitochondrial dysfunction. *J. Labelled Compd. Radiopharm.* **2005**, *48*, 131–137.
- (35) Min, J. J.; Biswal, S.; Deroose, C.; Gambhir, S. S. Tetraphenylphosphonium as a novel molecular probe for imaging tumors. *J. Nucl. Med.* **2004**, *45*, 636–643.
- (36) Steichen, J. D.; Weiss, M. J.; Elmaleh, D. R.; Martuza, R. L. Enhanced in vitro uptake and retention of <sup>3</sup>H-tetraphenylphosphonium by nervous system tumor cells. *J. Neurosurg.* **1991**, *74*, 116–122.
- (37) Cheng, Z.; Winant, R. C.; Gambhir, S. S. A new strategy to screen molecular imaging probe uptake in cell culture without radiolabeling using matrix-assisted laser desorption/ionization time-of-flight mass spectrometry. *J. Nucl. Med.* **2005**, *46*, 878–886.
- (38) Blower, P. J.; Lewis, J. S.; Zweit, J. Copper radionuclides and radiopharmaceuticals in nuclear medicine. *Nucl. Med. Biol.* **1996**, *23*, 957–980.
- (39) Reichert, D. E.; Lewis, J. S.; Anderson, C. J. Metal complexes as diagnostic tools. *Coord. Chem. Rev.* **1999**, *184*, 3–66.
- (40) Liu, S.; Edwards, D. S. Bifunctional chelators for therapeutic lanthanide radiopharmaceuticals. *Bioconjugate Chem.* **2001**, *12*, 7–34.
- (41) Liu, S. The role of coordination chemistry in development of target-specific radiopharmaceuticals. *Chem. Soc. Rev.* **2004**, *33*, 445–461.
- (42) Bähr, O.; Wick, W.; Weller, M. Modulation of MDR/MRP by wild-type and mutant p53. *J. Clin. Invest.* **2001**, *107*, 643–645.
- (43) Bähr, O.; Rieger, J.; Duffner, F.; Meyermann, R.; Weller, M.; Wick, W. P-glycoprotein and multidrug resistance-associated protein mediate specific patterns of multidrug resistance in malignant glioma cell lines, but not in primary glioma cells. *Brain Pathol.* **2003**, *13*, 482–494.
- (44) Yang, C. T.; Li, Y. X.; Liu, S. Synthesis and structural characterization of complexes of a DO3A-conjugated triphenylphosphonium cation with diagnostically important metal ions. *Inorg. Chem.*, in press.
- (45) Shannon, R. D. Revised effective ionic radii and systematic studies of interatomic distances in halides and chalcogenides. *Acta Crystallogr. Sect. A.* **1976**, *32*, 751–767.
- (46) Acampa, W.; Di, Benedetto, C.; Cuocolo, A. An overview of radiotracers in nuclear cardiology. *J. Nucl. Cardiol.* **2000**, *7*, 701–707.
- (47) Dilsizian, V. The role of myocardial perfusion imaging in vascular endothelial dysfunction. *J. Nucl. Cardiol.* **2000**, *7*, 180–184.
- (48) Schwaiger, M.; Melin, J. Cardiological applications of nuclear medicine. *Lancet* **1999**, *354*, 661–666.
- (49) Beller, G. A.; Zaret, B. L. Contributions of nuclear cardiology to diagnosis and prognosis of patients with coronary artery disease. *Circulation* **2000**, *101*, 1468–1478.
- (50) Parker, J. A. Cardiac nuclear medicine in monitoring patients with coronary heart disease. *Semin. Nucl. Med.* **2001**, *31*, 223–237.
- (51) Saha, G. B.; Go, R. T.; Macintyre, W. J. Radiopharmaceuticals for cardiovascular imaging. *Nucl. Med. Biol.* **1992**, *19*, 1–20.
- (52) Jain, D. Technetium-99m labeled myocardial perfusion imaging agents. *Semin. Nucl. Med.* **1999**, *29*, 221–236.
- (53) Piwnica-Worms, D.; Kronauge, J. F.; Chiu, M. L. Uptake and retention of hexakis(2-methoxyisobutylisoutrile) technetium(I) in cultured chick myocardial cells: mitochondrial and plasma membrane potential dependence. *Circulation* **1990**, *82*, 1826–1838.
- (54) Carvalho, P. A.; Chiu, M. L.; Kronauge, J. F.; Kawamura, M.; Jones, A. G.; Holman, B. L.; Piwnica-Worms, D. Subcellular distribution and analysis of technetium-99m-MIBI in isolated perfused rat hearts. *J. Nucl. Med.* **1992**, *33*, 1516–1522.
- (55) Crane, P.; Laliberte, R.; Heminway, S.; Thoolen, M.; Orlandi, C. Effect of mitochondrial viability and metabolism on technetium-99m-sestamibi myocardial retention. *Eur. J. Nucl. Med.* **1993**, *20*, 20–25.
- (56) Liu, S.; He, Z. J.; Hsieh, W. Y.; Kim, Y. S. Evaluation of novel cationic <sup>99m</sup>Tc-nitrido complexes as radiopharmaceuticals for heart imaging: Improving liver clearance with crown ether groups. *Nucl. Med. Biol.* **2006**, *33*, 419–432.
- (57) He, Z. J.; Hsieh, W. Y.; Kim, Y. S.; Liu, S. Evaluation of novel cationic <sup>99m</sup>Tc(I)-tricarbonyl complexes as potential radiotracers for myocardial perfusion imaging. *Nucl. Med. Biol.* **2006**, *33*, 1045–1053.
- (58) Kim, Y. S.; He, Z. J.; Hsieh, W. Y.; Liu, S. Impact of bidentate chelators on lipophilicity, stability and biodistribution characteristics of cationic <sup>99m</sup>Tc-nitrido complexes. *Bioconjugate Chem.* **2007**, *18*, 929–936.
- (59) Liu, S. Ether and crown ether-containing cationic <sup>99m</sup>Tc complexes useful as radiopharmaceuticals for heart imaging. *Dalton Trans.* **2007**, 1183–1193.
- (60) Fantin, V. R.; Berardi, M. J.; Scorrano, L.; Korsmeyer, S. J.; Leder, P. A novel mitochondriotoxic small molecule that selectively inhibits tumor cell growth. *Cancer Cell* **2002**, *2*, 29–42.
- (61) Britten, C. D.; Rowinsky, E. K.; Baker, S. D.; Weiss, G. R.; Smith, L.; Stephenson, J.; Rothenberg, M.; Smetzer, L.; Cramer, J.; Collins, W.; Von, Hoff, D. D.; Eckhardt, S. G. A phase I and pharmacokinetic study of the mitochondrial-specific rhodacyanine dye analog MKT-077. *Clin. Cancer Res.* **2000**, *6*, 42–49.
- (62) Kandela, I. K.; Bartlett, J. A.; Indig, G. L. Effect of molecular structure on the selective phototoxicity of triarylmethane dyes towards tumor cells. *Photochem. Photobiol. Sci.* **2002**, *1*, 309–314.
- (63) Kandela, I. K.; Lee, W.; Indig, G. L. Effect of the lipophilic/hydrophilic character of cationic triarylmethane dyes on the selective phototoxicity toward tumor cells. *Biotech. Histochem.* **2003**, *78*, 157–169.
- (64) Trapp, S.; Horobin, R. W. A predictive model for the selective accumulation of chemicals in tumor cells. *Eur. Biophys. J. Biophys. Lett.* **2005**, *34*, 959–966.
- (65) Horobin, R. W. Uptake, distribution, and accumulation of dyes and fluorescent probes with living cells: a structure-activity modeling approach. *Adv. Colour Sci. Technol.* **2001**, *4*, 101–107.
- (66) Márián, T.; Balkay, L.; Szabó, G.; Krasznai, Z. T.; Herádi, Z.; Galuska, L.; Szabó-Péli, J.; Ésik, O.; Trón, L.; Krasznai, Z. Biphasic accumulation kinetics of [<sup>99m</sup>Tc]-hexakis-2-methoxyisobutyl isoutrile in tumour cells and its modulation by lipophilic P-glycoprotein ligands. *Eur. J. Pharm. Sci.* **2005**, *25*, 201–209.
- (67) Márián, T.; Szabó, G.; Nagy, H.; Szincsák, N.; Juhász, I.; Galuska, L.; Balkay, L.; Mikecz, P.; Trón, L.; Krasznai, Z. In vivo and in vitro multitracer analysis of P-glycoprotein expression-related multidrug resistance. *Eur. J. Nucl. Med. Mol. Imaging* **2003**, *30*, 1147–1154.
- (68) Lorke, D. E.; Krüger, M.; Buchert, R.; Bohuslavizki, K. H.; Clausen, M.; Schumacker, U. In vitro and in vivo tracer characteristics of an established multidrug-resistant human colon cancer cell line. *J. Nucl. Med.* **2001**, *42*, 646–654.

JM0704088